Gusev crater: Wind-related features and processes observed by the Mars Exploration Rover Spirit

Ronald Greeley,[1] R. E. Arvidson,[2] P. W. Barlett,[3] Diana Blaney,[4] N. A. Cabrol,[5] P. R. Christensen,[1] R. L. Fergason,[1] M. P. Golombek,[4] G. A. Landis,[6] M. T. Lemmon,[7] S. M. McLennan,[8] J. N. Maki,[4] Timothy Michaels,[9] J. E. Moersch,[10] L. D. V. Neakrase,[1] S. C. R. Rafkin,[9] Lutz Richter,[11] S. W. Squyres,[12] P. A. de Souza Jr.,[13] R. J. Sullivan,[12] S. D. Thompson,[1] and P. L. Whelley[1]

Received 11 May 2005; revised 23 September 2005; accepted 5 October 2005; published 6 January 2006.

[1] Wind-related features observed by the rover Spirit in Gusev crater, Mars, include patches of soil on the surface, some of which are organized into bed forms. Windblown grains include dust (inferred to be <3 μm in diameter), sands (up to a few hundred μm in diameter), and granules (>2 mm in diameter). Microscopic Imager data show the sands and granules to be rounded and relatively spherical, typical of grains transported long distances by the wind. The interior of bed forms exposed by rover operations suggests the infiltration of dust among the grains, indicating that these sands are not currently experiencing saltation. Orientations of 1520 features (such as bed forms and ventifacts) along Spirit's traverse from the landing site (the Columbia Memorial Station) to West Spur in the Columbia Hills suggest primary formative winds from the north-northwest, which correlate with measurements of features seen in orbiter images and is consistent with afternoon winds predicted by atmospheric models. A secondary wind from the southeast is also suggested, which correlates with predictions for nighttime/early morning winds. Wind abrasion is indicated by ventifacts in the form of facets and grooves cut into rocks, the orientations of which also indicate prevailing winds from the north-northwest. Orientations of many aeolian features in the West Spur area, however, have more scatter than elsewhere along the traverse, which is attributed to the influence of local topography on the patterns of wind. Active dust devils observed on the floor of Gusev from the Columbia Hills demonstrate that dust is currently mobile. Sequential images of some dust devils show movement as rapid as 3.8 m/s, consistent with wind velocities predicted by atmospheric models for the afternoon, when most of the dust devils were observed. Sands accumulated on the rover deck in the same period suggest that some sands in the Columbia Hills experience active saltation. "Two-toned" rocks having a light band coating at their bases are considered to represent partial burial by soils and subsequent exposure, while "perched" rocks could represent materials lowered onto other rocks by deflation of supporting soils. Measurements of the heights of the light bands and the perched rocks range from <1 cm to 27 cm, indicating local deflation by as much as 27 cm.

Citation: Greeley, R., et al. (2006), Gusev crater: Wind-related features and processes observed by the Mars Exploration Rover Spirit, *J. Geophys. Res.*, *111*, E02S09, doi:10.1029/2005JE002491.

[1]Department of Geological Sciences, Arizona State University, Tempe, Arizona, USA.
[2]Earth and Planetary Sciences, Washington University, St. Louis, Missouri, USA.
[3]Honeybee Robotics, New York, New York, USA.
[4]Jet Propulsion Laboratory, California Institute of Technology, Pasadena, California, USA.
[5]NASA Ames Research Center, Moffett Field, California, USA.
[6]NASA Glenn Research Center, Cleveland, Ohio, USA.
[7]Department of Atmospheric Sciences, Texas A&M University, College Station, Texas, USA.
[8]Department of Geosciences, State University of New York at Stony Brook, Stony Brook, New York, USA.
[9]Southwest Research Institute, Boulder, Colorado, USA.
[10]Department of Earth and Planetary Sciences, University of Tennessee, Knoxville, Tennessee, USA.
[11]Institut für Raumsimulation, Deutschen Zentrum für Luft- und Raumfahrt, Cologne, Germany.
[12]Department of Astronomy, Cornell University, Ithaca, New York, USA.
[13]CVRD Group, Vitória, Brazil.

0148-0227/06/2005JE002491$09.00

1. Introduction

[2] The floor of Gusev crater was selected as the landing site for the Mars Exploration Rover Spirit [*Arvidson et al.*, 2006]. Previous orbital analyses of this ~160 km impact crater have shown a complex geologic history that includes potential modification by mass wasting, fluvial activity, volcanism, and extensive aeolian (i.e., wind) processes [*Kuzmin et al.*, 2000; *Cabrol et al.*, 2003; *Golombek et al.*, 2003, 2005; *Greeley et al.*, 2003, 2004, 2005b].

[3] In this report we document wind-related features observed in the operational area of Spirit from the time of landing on the first sol through sol 312 (3 January 2004 through 18 November 2004; this corresponds to L_s 327.7° to 116.8°, or southern summer to southern winter). We discuss observations at the landing site, designated the Columbia Memorial Station (CMS) [*Squyres et al.*, 2004] and along the ~4 km traverse into the western flank of the Columbia Hills, called West Spur (Figure 1). We also discuss observations of active aeolian processes postsol 312 and the relationships of the observed aeolian surface features to those seen from orbit and to wind vectors predicted by models of the atmosphere. Following the geological convention, our wind directions are given in azimuths toward which the wind blows.

[4] Various wind-related features and their dimensions can be identified from the surface observations (Figures 2 and 3). These include bed forms (such as ripples), drift deposits associated with rocks, erosional and abraded features such as ventifacts, and features such as "perched" rocks suggestive of wind deflation. In addition, fine-grained materials (sand and dust) are analyzed in bed forms and as patches on the surface. We use the term "soil" for these materials, following the convention of *Squyres et al.* [2004] for unconsolidated grains on or near the surface.

[5] We first discuss the analytical approach and data sets used for the study, then describe the wind-related features seen from the surface by Spirit and from orbit over the rover operations area. We then discuss the wind regime derived from the observations and as modeled, for comparisons with the surface features. Finally, we discuss the implications of the results for the geology of Gusev crater, and outline some of the key problems that remain to be resolved.

2. Analytical Approach

[6] Images and other Spirit data relevant for aeolian features were analyzed for the types and occurrences of features as functions of terrain in five zones along the traverse (Figure 1). As described by *Grant et al.* [2004], the bedrock geology of the floor of Gusev crater appears to consist of basaltic rocks [*McSween et al.*, 2004] which were probably emplaced as very fluid lava flows ~3.5 Gy ago [*Greeley et al.*, 2005a], thus establishing an older age limit for the surficial geology, including aeolian features.

[7] Zone 1 (sols 1 through 61, L_s 327.7–360.0) includes the immediate landing site, CMS, and the traverse to the approximate edge of the ejecta blanket from Bonneville crater. This zone lies within a relatively dark linear wind streak seen on the surface from orbit that is inferred to be the track left by the passage of a dust devil [*Greeley et al.*, 2004]. Zone 2 (sols 62 through 109, L_s 0.5–23.8) is on the ejecta deposits from Bonneville and Missoula craters. It extends from the edge of zone 1 to the rim of Bonneville crater, then down the outbound traverse to the outer southeast edge of the ejecta from Missoula crater. This zone is within bright ejecta deposits, as seen from orbit. Zone 3 (sols 110 through 155, L_s 24.2–45.2) is from the end of zone 2 across the plains to West Spur at the base of the Columbia Hills. This zone consists primarily of plains materials, but also includes some ejecta from small craters. Zone 4 (sols 156 through 193, L_s 45.7–62.5) is the transitional area between the plains and West Spur. It includes a shallow moat-like area at the base of the hills, as detected on rover-derived topography [*Li et al.*, 2005]. Zone 5 (sols 194 through 312, L_s 62.9–116.8) is the traverse up West Spur and along the connecting ridge to the main Columbia Hills complex. Although most of the rocks on the West Spur are loose fragments, a few bedrock exposures were encountered.

[8] As summarized by *Arvidson et al.* [2006], the Columbia Hills have a relief of about 120 m over a lateral distance of 2–3 km. Observations from Spirit indicate that the hills are composed of granular rocks that are layered, with layers tending to be conformable with topography [*Squyres et al.*, 2006]. The rocks appear to be poorly sorted and composed of pyroxene, hematite, magnetite, and basaltic glass. Some of the rocks exhibit evidence for goethite. Most of the rocks encountered are "float" underlain and surrounded by soils, although some bedrock has also been encountered. Enhanced values of sulfur, halides, and, in some cases, phosporus, relative to the plains olivine-bearing basalts argue for aqueous alteration of the hills rocks. Soils in the hills have textures, compositions, and minerals essentially identical to the basaltic soils found in the plains. These similarities argue that winds have homogenized the soils to first order over distances that exceed the ~4 km traverse covered by Spirit. Moreover, thin dust deposits cover soils and rocks in the hills in much the same manner as was found in the plains.

2.1. Image Analysis

[9] Images from the Pancam [*Bell et al.*, 2003], Navcam, and Hazcam [*Maki et al.*, 2003] were searched for features indicative of wind processes. Each feature was classified by type (e.g., ripples) and measurements taken of specific parameters such as ripple length and azimuth. In addition, *Golombek et al.* [2005] obtained counts of rocks 0.05 to 2 m in diameter for ~70° sectors of panoramas within 10 m of the rover at the CMS, at the boundary of zones 1 and 2, and near the rim of Bonneville crater (zone 2). These data were used to derive estimates of the aerodynamic roughness parameter, z_0 (Table 1). Higher values of z_0 (due to larger and/or more densely distributed rocks) indicate that a larger fraction of wind shear stress will be absorbed by these roughness elements, resulting in a smaller fraction of shear stress available to move loose grains on the surface between the roughness elements [*Gillette and Stockton*, 1989; *Raupach et al.*, 1993; *Nickling and McKenna Neuman*, 1995]. Grain movement could be retarded through these areas, leading to greater abundances of drifts associated with roughness elements. This is evidenced by the increased frequency of bed forms in zone 2 compared to zone 3.

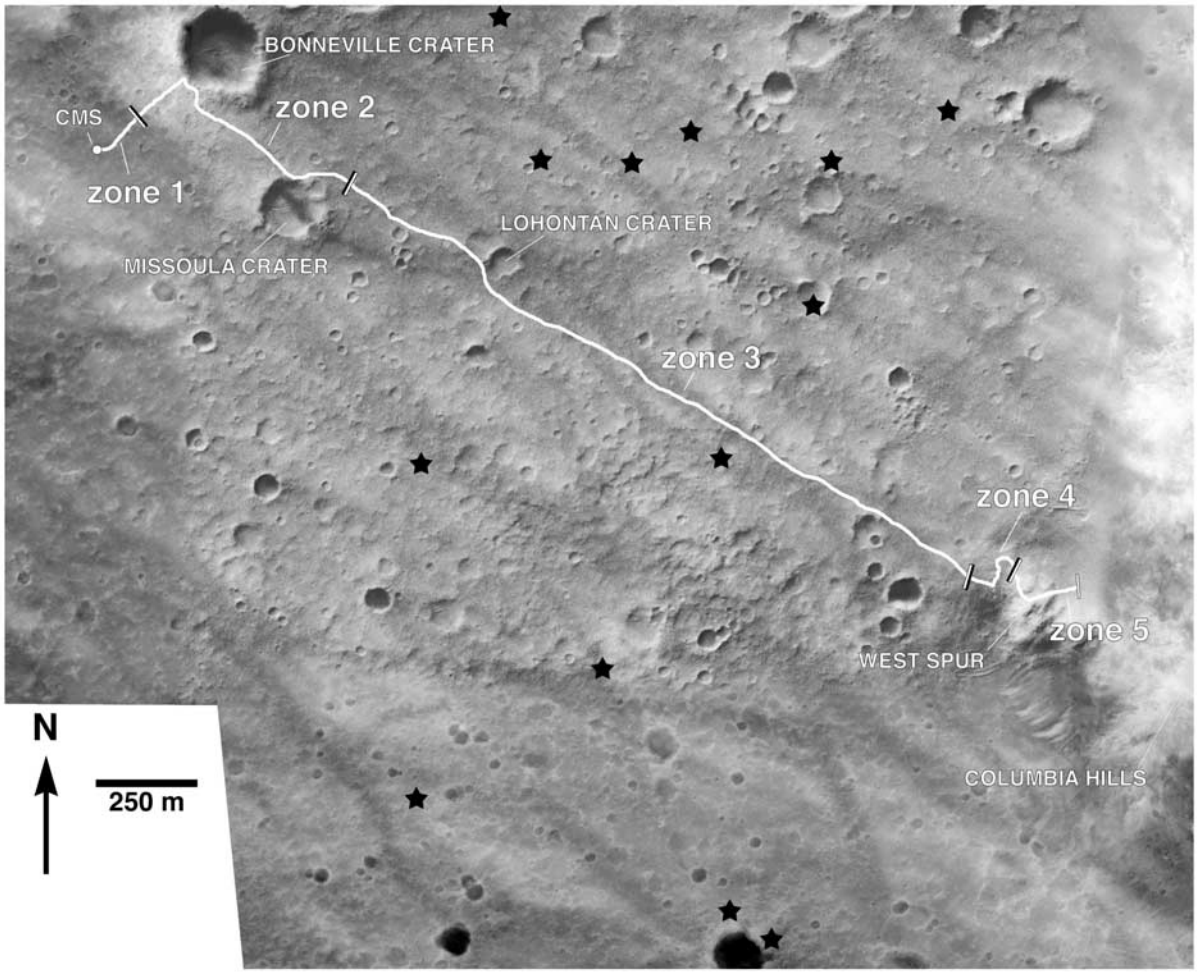

Figure 1. Mars Orbiter Camera mosaic showing the Spirit landing site (CMS is the Columbia Memorial Station), the rover traverse to the Columbia Hills, and the identification of zones used for analysis of wind-related features. The linear dark wind streaks trending northwest-southeast are considered to be tracks left by the passage of dust devils, the orientations of which are consistent with the modeled prevailing wind directions. Stars indicate the approximate location of some of the active dust devils imaged by Spirit from the Columbia Hills.

[10] The frequency distributions of aeolian features were normalized by surface area of the scenes imaged. Most of the Navcam and Hazcam images were taken in middle to late afternoon, so the illumination was generally consistent. However, the orientation of the rover with respect to illumination was not consistent, a factor that is particularly significant for the Hazcams, which are fixed to the rover body. Also, the Pancam frames were not always taken at the same time of day. In addition, the Pancam frames tended to be acquired with viewing toward the southeast, giving a somewhat biased view of the northwest sides of rocks. The extent of soil patches (areas that lack organized bed forms, wind tails, rocks and bedrock) were determined using polar-projected Navcam images; however, rocks smaller than ~15 cm across were often difficult to discern and they are included in the soil patch category.

[11] Images from the Microscopic Imager (MI) [*Herkenhoff et al.*, 2003] were analyzed for soils on the surface and in the subsurface where exposed by rover wheel operations [*Herkenhoff et al.*, 2004]. Grain size frequency distributions were determined from the MI frames and the longest and shortest axes of individual grains were measured. We follow the Wentworth Grade Scale [*Wentworth*, 1922] for the classification and sizes of the grains (Table 2). The MI images have a pixel scale of 31 μm/pixel [*Herkenhoff et al.*, 2003] and in some high-quality images we can identify individual grains as small as 120 μm in diameter. However, for grain size distributions and shapes, only grains >200 μm in diameter (fine sands and larger) could be analyzed with confidence. As discussed previously [*Arvidson et al.*, 2004], the texture of soils where compacted by the Mössbauer spectrometer plate suggests the presence of very fine grains, inferred to be dust or weakly bonded dust aggregates. Martian dust in the atmosphere is considered to be composed of particles ~3 μm in diameter, based on the optical properties [*Lemmon et al.*, 2004].

2.2. Miniature Thermal Emission Spectrometer (MiniTES) Data

[12] The Miniature Thermal Emission Spectrometer (MiniTES) provides remote sensing information on the

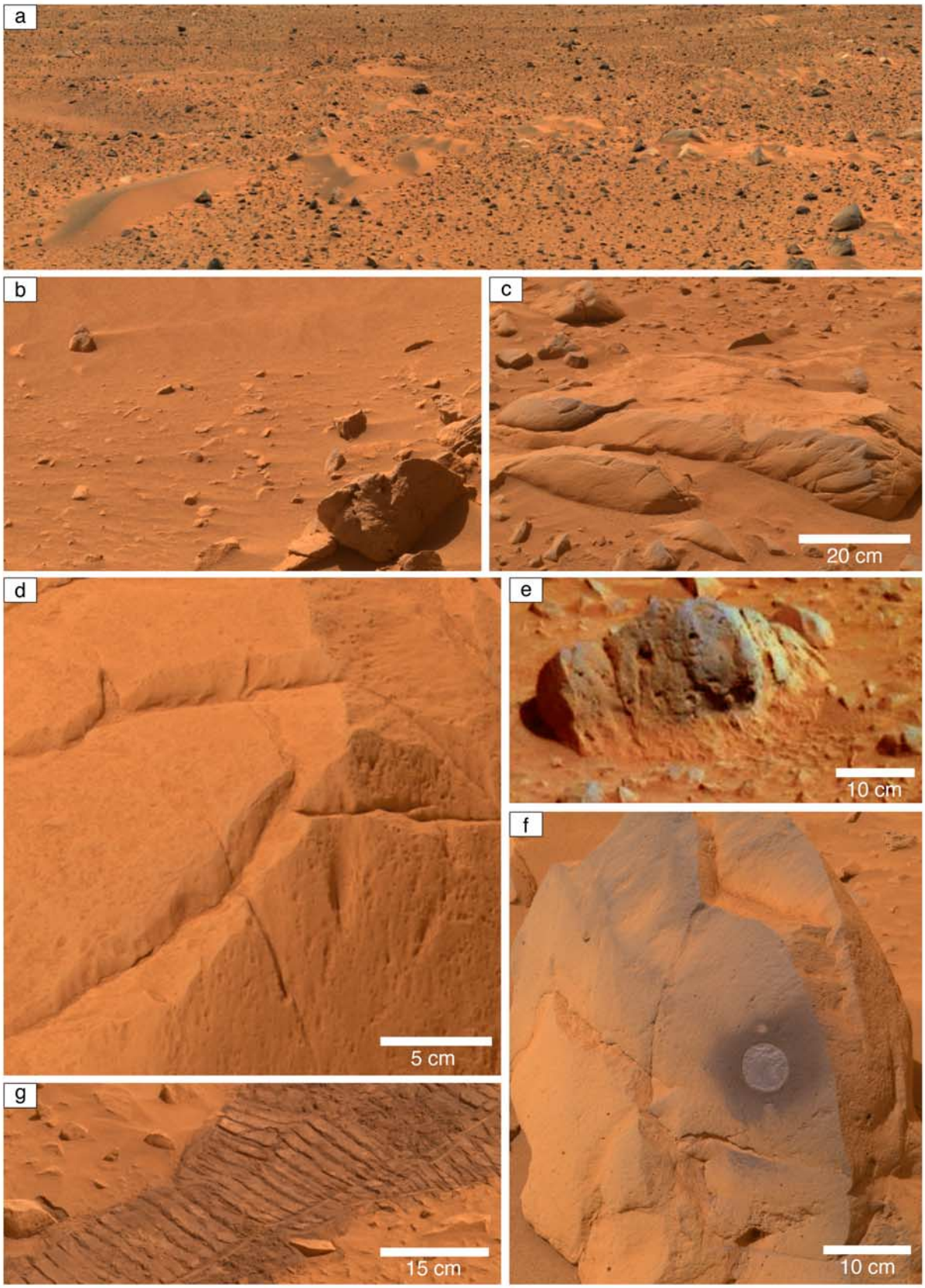

Figure 2

mineralogy and physical properties of soils and rocks [*Christensen et al.*, 2003], and is especially important for assessing materials that are not in the immediate vicinity of the rover. Thermal inertia data were derived from MiniTES measurements acquired at multiple times during the day. The measured radiance was converted to a target temperature, which approximates the surface kinetic temperature. These temperatures were then used to determine the thermal inertia. Particle sizes were inferred using the technique described by *Presley and Christensen* [1997] and the results were compared to particle sizes measured directly in MI images where available. When deriving particle sizes from thermal inertia measurements, an atmospheric pressure of 600 Pascals was used (Martian atmospheric pressure at −1.5 km, the elevation of the landing sites, and L_s 0° (from *Smith and Zuber* [1998]) and combined bulk density and specific heat of 1.0×10^6 J/m3 [*Neugebauer et al.*, 1971]. Initial thermal inertia results at Gusev were reported by *Christensen et al.* [2004a] and *Golombek et al.* [2005]. Thermal inertia values given here differ slightly from those initial results due to improvements in the MiniTES instrument calibration, the inclusion of Pancam dust opacity measurements as model input parameters, varying both albedo and inertia to fit diurnal temperature curves, and the use of full diurnal temperature measurements rather than nighttime data only. These differences, however, do not significantly change the geologic interpretation.

2.3. Orbiter Data

[13] Mars Orbiter Camera (MOC) [*Malin and Edgett*, 2001] images from Mars Global Surveyor (MGS) were analyzed to determine the orientations of wind-related features in the general area of Spirit operations. All MOC Narrow Angle images taken from April 1999 to October 2003 were analyzed for an area 20 by 20 km centered on CMS. All of the images analyzed were taken through a red equivalent filter (500–900 nm) and have resolutions of 1.4 to 7.1 m/pixel. In addition, Thermal Emission Imaging System (THEMIS) [*Christensen et al.*, 2004b] data from Mars Odyssey and High Resolution Stereo Camera (HRSC) [*Neukum et al.*, 2004] images from Mars Express were analyzed to identify potential changes on the surface just before and during Spirit operations [*Greeley et al.*, 2005b].

2.4. Atmospheric Modeling Predictions

[14] Results from two atmospheric models were used to predict wind patterns for comparisons with the aeolian features. The NASA Ames Mars General Circulation Model (MGCM) simulates the mean atmosphere of Mars with a standard simulation grid spacing of 9.0° in longitude by 7.5° in latitude [*Pollack et al.*, 1990; *Haberle et al.*, 1993]. Thus the MGCM predicts wind patterns over large areas to provide an assessment of the general wind regime. The Mars Regional Atmospheric Modeling System (MRAMS) [*Rafkin et al.*, 2001] is used to predict finer-scale winds, and was used to model winds in Gusev crater in support of MER landing site selection [*Rafkin and Michaels*, 2003] and for comparison with surface features [*Greeley et al.*, 2003]. MRAMS is a nonhydrostatic, fully compressible mesoscale atmospheric model, which employs "nested" grid cells for enhanced resolution over areas of interest. The model uses MGCM results for lateral boundary conditions, and surface characteristics derived from MGS, including Mars Orbiter Altimeter (MOLA) 1/32° gridded topography, Thermal Emission Spectrometer thermal inertia [*Putzig et al.*, 2005] and albedo at 1/20° and 1/8° resolution, respectively.

3. Observations From Spirit

[15] Pancam views (Figures 2a and 3a) from Spirit across the floor of Gusev crater show a terrain dominated by loose basaltic rocks, inferred to be ejecta from impact craters, set in a matrix of soils that have probably been emplaced by aeolian processes [*Squyres et al.*, 2004; *Grant et al.*, 2004]. In this section we classify and describe the deposits of windblown materials and the rocks that appear to have been subjected to aeolian processes.

3.1. Wind Depositional Features

[16] Deposits of windblown materials occur in organized bed forms (such as ripples), drifts, wind tails, patches of soil on the surface, and as dust settled from the atmosphere, which typically forms a veneer on the tops of rocks and the soils. Soil deposits and bed forms are more frequent on the floors of impact craters, such as Bonneville, and within shallow circular depressions, or "hollows," that are inferred to be small, highly degraded impact craters partly filled with windblown material (Figure 3a) [*Grant et al.*, 2004, 2006; *Golombek et al.*, 2006].

3.1.1. Soils

[17] In general, the soils consist of five components (Figure 4): (1) bright dust, (2) a monolayer of coarse sands and granules (0.5 to a few mm in diameter), (3) subangular lithic fragments several mm or larger in length, (4) a cohesive crust as thick as several mm beneath the dust and coarse grains, and (5) dark soil (Figure 2g). Not all of these materials are present in all locations [*Yen et al.*, 2005].

[18] The bright dust deposits (Figure 2f) form a veneer that is inferred to be thinner than a mm and to consist of particles a few μm in diameter that settled from the atmosphere. It has the same visible to near-IR spectral properties as the material that settled on the rover deck and the material observed on tops of rocks. The monolayer of coarse grains, where present, forms a surface "armor" (Figure 4b) considered to be a lag deposit of windblown material that is probably transported in traction, or creep, by

Figure 2. Pancam views: (a) toward the northeast from CMS showing rocky surface and bed forms, including "Snake," the 2.6-m-long bed form on the left, (b) small wind tails formed in the lee of rocks seen on sol 290 (L_s 106.4°) in zone 5, (c) rocks imaged on sol 107 (L_s 22.8°) (zone 2) showing ventifact grooves, (d) closeup of ventifact grooves on rock face, imaged on sol 73 (L_s 6.1°) in zone 2, (e) "two-toned" rock, typified by the light zone at the base of the rock, imaged on sol 108 (L_s 23.3°) in zone 2, (f) circular zone abraded by the RAT on the rock "Humphrey," showing the dark debris shed from the RAT onto the brighter red dust covering the rock, imaged on sol 60 (L_s 359.5°) in zone 1, and (g) multiple wheel tracks left by Spirit as imaged on sol 89 (L_s 14.0°) in zone 2, showing darker soil beneath bright dust on the surface.

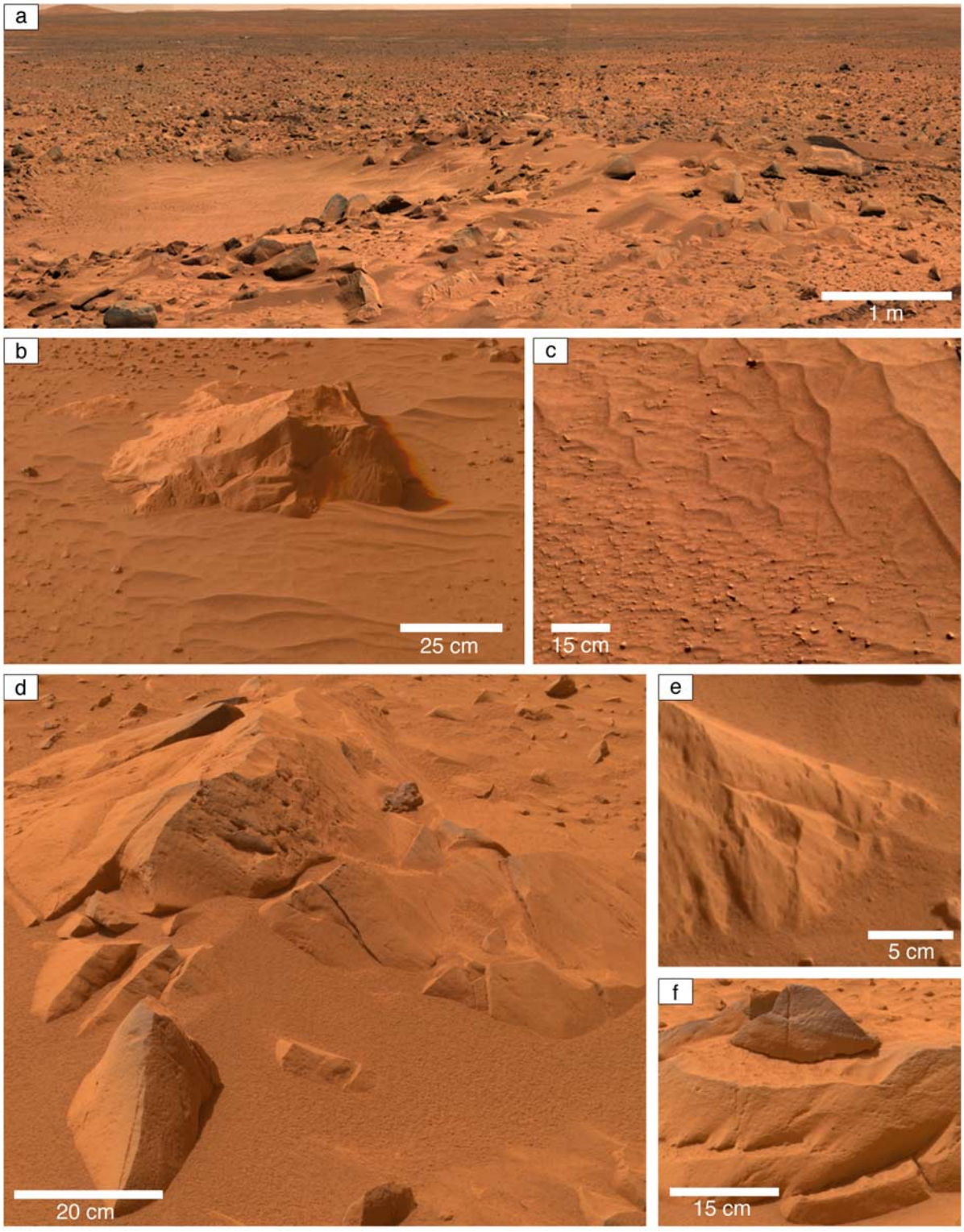

Figure 3. Pancam views: (a) across a small "hollow" toward CMS (southeast) imaged on sol 69 (L_s 4.1°) in zone 2, showing accumulation of windblown sediments in the depression and as bed forms on the rim (note wheel track across bed form), (b) the rock "Toad" in "Laguna Hollow," imaged on sol 53 (L_s 355.9°) in zone 1, showing small ripples, (c) bed forms inferred to be ripples and very small wind tails associated with pebbles imaged on sol 56 (L_s 357.5°) in zone 1, (d) ventifact facets showing characteristic sharp crest where two facets meet, imaged on sol 99 (L_s 18.9°) in zone 2, (e) ventifact grooves that appear to be partly buried by soils, imaged on sol 87 (L_s 13.1°) in zone 2, and (f) "perched" rock on top of the rock "Terrace," imaged on sol 63 (L_s 1.0°) in zone 2.

Table 1. Rock Distributions and Derived Aerodynamic Roughness, z_0

Zone	Name	Area, m^2	Number of Rocks	Rock Coverage, %	Largest Rock, m	Aerodynamic Roughness, cm
1	Mission Success	57	1089	7	0.5	0.004
2	Legacy	58	426	5	0.8	0.12
2	Bonneville	84	689	29	1.3	0.14

the impact of smaller saltating grains. The larger lithic fragments might also represent material that could be moved in surface traction (Figure 4c). Some soils that have been disturbed by the rover wheels break into small slabs, or plates, a few mm thick and as large as 15 cm across (Figure 4d) (L. Richter et al., manuscript in preparation, 2006). This behavior is interpreted to represent the presence of a crust of cohesive material, either by cementation or electrostatic bonding. Dark soils are found beneath the surface material, wherever the rover wheels or the Instrument Deployment Device (IDD) operations have disturbed them (Figures 2g and 4e).

[19] Clastic materials such as sand are commonly described on Earth on the basis of their size distributions, grain roundness, grain shape, and other parameters [*Pettijohn et al.*, 1987]. Size distributions are typically determined by sieving samples into size fractions and applying statistical measures to the results. Particularly important are the central tendency (such as the mean), maximum size, sorting (dispersion around the central tendency), and presence of more than one central tendency, such as bimodality. These and other parameters provide information on the history of the deposits and the processes involved in their emplacement. Although a complete sedimentary analysis of soils at Gusev cannot be made with available data, MI images provide a surrogate for some of these parameters.

[20] Some of the soils imaged by the MI have a bimodal size distribution of coarse grains in a matrix of fine grains too small to be resolved by the MI, but inferred to be dust or aggregates of dust grains. MI images (Figures 5 and 6) were taken of soils: (1) on two bed forms (Drifter and Arena), (2) nonorganized soil (Ramp Flats), and (3) the bed form, Serpent (where the surface was disrupted to expose the subsurface materials). Drifter and Arena have a surface monolayer of coarse grains 1 to 2 mm in diameter that appear to be well sorted (Figure 7). We suggest that this monolayer represents a lag deposit that armors the surface of the bed form near the crest, similar to that observed by *Sharp* [1963] in the Mojave Desert. The coarse clasts in Ramp Flats range in size from 0.25 to >9 mm, and are very poorly sorted. The size distribution revealed in the disturbed interior of Serpent shows a bimodal (or trimodal, taking into account the inferred dust) distribution centered at about 1.4 mm and 0.35 mm. The coarser mode is represented by particles of the coarse sand and granule armor, which are considered to have slid into the depression left by the rover left front wheel. We suggest that this distribution reflects the overall composition of the undisturbed bed form interior to include fine sand and infiltrated dust. Unfortunately, data do not allow the determination of the amounts of dust and fine sand present in the bed form as a whole. However, the presence of the infiltrated dust suggests that the particles in the bed form do not currently experience saltation because the dust would have been "cleansed" from the sands in the process. Furthermore, the coarse-grained armor of a monolayer of particles covering the bed form exhibits signs of interparticle induration in the form of fracture lines where they have been disturbed by the rover, similar to crusts observed in nonorganized soils (L. Richter et al., manuscript in preparation, 2006). Thus the Serpent bed form is not considered to be currently active.

[21] Shape is typified by measurements of the long, short, and intermediate axes of the grains in an x, y, and z coordinate system, and is used assess parameters such as sphericity. Roundness is a parameter that refers to the curvature of the corners of grains. Both shape and roundness are commonly determined qualitatively in the field using comparison charts. On the basis of the chart of *Dutro et al.* [1989], MI data enable these parameters to be determined for the coarse grains observed in Gusev soils. The coarse grains in the bed forms are rounded to well rounded, and subprismoidal to spherical in shape. In combination with the high degree of sorting, these results are typical for grains that have been transported some distance (i.e., not from local sources), during which the corners were abraded and smoothed. In contrast, the coarse clastics in Ramp Flats are discoidal, suggesting that they are locally derived. Their roundness, however, shows that they have been abraded by a process that we suggest was the impact of saltating grains (i.e., "sand blasting") in the past.

[22] MiniTES temperature measurements and Pancam images provide additional information on the soils that were not accessed directly by the rover. Initial results indicate that the thermal inertia increases from the CMS toward Bonneville crater, ranging from 150 ± 25 to 450 ± 75 J m^{-2} K^{-1} $s^{-1/2}$ [*Christensen et al.*, 2004a; *Golombek et al.*, 2005], which probably reflects the increase in rocky ejecta toward the crater rim. Some of the lowest thermal inertia material was found in the hollows (Figure 3a). For example, Middle Ground Hollow has a thermal inertia of 150 ± 28 J m^{-2} K^{-1} $s^{-1/2}$ [*Fergason et al.*, 2006] corresponding to fine sand (Table 2) [*Presley and Christensen*, 1997]. The MiniTES thermal inertias for the soils average 175 ± 25 J m^{-2} K^{-1} $s^{-1/2}$ [*Fergason et al.*, 2006] along the traverse from CMS

Table 2. Abbreviated Wentworth Grade Scale for Small Clastic Particles Compared to "Dust" Diameters on Earth and Mars[a]

Diameter, mm	Particle	Diameter, μm
4–2	granule	4000–2000
2–1	very coarse sand	2000–1000
1–0.5	coarse sand	1000–500
0.5–0.25	medium sand	500–250
0.25–0.125	fine sand	250–125
0.125–0.0625	very find sand	125–62.5
0.0625–0.004	silt	62.5–4
<0.004	clay	<4

[a]Dust: Earth continental, 10–50 μm [*Pye*, 1987]; Earth intercontinental, μμ < 10 [*Pye*, 1987]; Mars atmosphere, ~3 μm [*Lemmon et al.*, 2004].

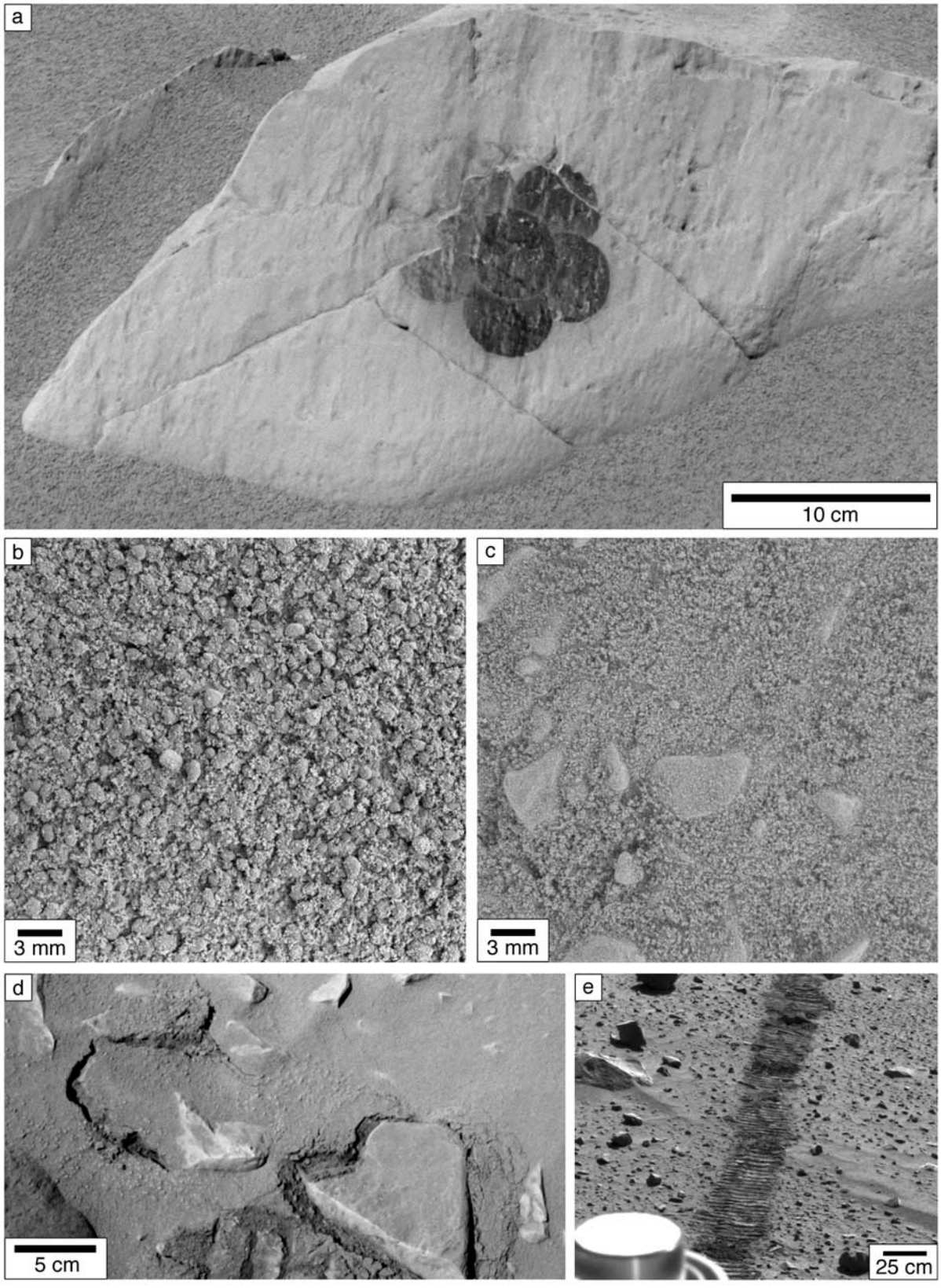

Figure 4

to Bonneville crater. These values are consistent with those calculated from THEMIS (270 ± 40 to 330 ± 50 J m^{-2} K^{-1} $s^{-1/2}$, average 306) and TES (315 ± 20 J m^{-2} K^{-1} $s^{-1/2}$) data obtained from orbit [*Golombek et al.*, 2005], suggesting a particle size of 500–3000 μm in soil patches [*Christensen et al.*, 2004a].

3.1.2. Bed Forms

[23] Bed forms, such as ripples and dunes, are deposits of sand and granule-size particles transported principally in saltation in flowing fluids and organized into regular patterns. Fluids can be wind, water, or dense mixtures of particles and gases, as in base surge deposits from volcanic eruptions or impact cratering events. The size, shape, and arrangements of bed forms, coupled with analyses of the particles and internal bedding structures, provide insight into the processes of formation, directions and distance of transport, and the potential sources of the grains of which they are composed. Smaller bed forms, such as ripples, often reflect wind conditions strongly influenced by local topography and can change patterns on timescales of minutes, whereas larger bed forms, such as large dunes, are indicative of wind patterns over larger areas and longer times. As reviewed by *Pye and Tsoar* [1990], windblown dunes require a supply of particles and winds of sufficient strength to move them, and for sufficient wind durations to lead to an organized deposit. Once formed, existing dunes may be remobilized as a consequence of increased wind activity and/or an influx of "fresh" particles, as during heavy spring time runoff when fluvial systems transport masses of clastic sediments. Consequently, dunes can be indicators of climate regime; for example, some dunes on Earth are not currently active and are considered to reflect past climates [*Livingstone and Warren*, 1996]. The lengths and orientations of bed form axes are defined by their crests, which for transverse features are orthogonal to the formational wind direction. Under unidirectional winds, bed forms are asymmetric in cross section, with the steeper slope ("slip face") on the downwind or leeward side. Thus the identification of the steep side of bed forms enables the determination of the formational wind direction. However, bed forms subjected to "reversing" winds (winds with two prevailing directions ~180° apart) tend to have symmetric cross sections, leading to ambiguity in the interpretation of the formational wind direction.

[24] In principle, dunes can be distinguished from ripples by grain size distributions; dunes generally have finer grains along the crest in comparison to the area between dunes (i.e., the troughs), whereas ripples tend to have coarser grains on their crest in comparison to the grains in the troughs. MI images were obtained on the crest and in the trough of only one bed form in Gusev, named Arena (Figure 5). The size distribution of grains measured on the MI images show that coarser grains occur on the crest (Figure 7) and we conclude that Arena and most of the similar bed forms are ripples [*Greeley et al.*, 2004]. Consequently, the orientations of these features may be more indicative of local, topographically induced wind patterns than of regional-scale patterns.

[25] Bed forms are common in all five zones in Gusev, but have a lower frequency in zone 3 (Figure 8). Their crest lengths range from a few cm to 16 m (Figures 3a, 3b, and 9) with most <2 m long. Although some occur in sets with wavelengths <0.5 m, most are found as isolated structures set within soil patches. Some of the larger bed forms are thought to be small dunes or complex ripples that have merged to form a larger mass, as shown in Figure 9.

[26] Some features seen from orbit and in the distance from Spirit have the appearance of dunes (i.e., could be dune forms). For example, Bonneville crater [*Golombek et al.*, 2006, Figure 19] contains dune-like features on its floor. These large bed forms were not examined in situ but were observed by MiniTES remotely, and from these measurements a thermal inertia of 160 ± 35 to 200 ± 40 J m^{-2} K^{-1} $s^{-1/2}$ was calculated [*Fergason et al.*, 2006], corresponding to a particle size of ~60 to 160 μm, or fine sand [*Presley and Christensen*, 1997].

[27] The orientations of bed form crests (Figure 10) in the five zones are generally consistent and indicate formative winds from either the north-northwest or south-southeast. Bed form cross sections were assessed qualitatively; of the 387 features identified, ~30 are considered to be asymmetric, ~50 are symmetric, and the remainder have insufficient data for determination. The orientations of the asymmetric bed forms suggests formative winds from the north-northwest. In addition, a topographic map was constructed for Serpent (Figure 6), which shows it to be slightly asymmetric and consistent with the formative winds from the northwest, although the steep downwind side of the bed form suggests the possibility of a reversing wind.

[28] Several bed forms were crossed by the rover, which left wheel depressions, revealing the dark soil component (Figures 2g and 4e). MI images of these areas suggest the presence of sand and dust in the dark soil. In most cases the surfaces of the bed forms did not fracture to form the platey clods that would be indicative of a cohesive crust.

[29] Bed forms viewed by MiniTES have thermal inertias of 160 to 250 J m^{-2} K^{-1} $s^{-1/2}$, suggesting particle sizes of 60–400 μm in diameter, in agreement with particle sizes measured on MI images. MI data show a bimodal size distribution with modes centered on fine sand (0.1–0.3 mm) and coarse sand to granules (1–3 mm) [*Herkenhoff et al.*, 2004].

3.1.3. Drift Deposits (Wind Tails)

[30] Deposits of windblown material occur around some rocks as elongated triangular-shaped masses called wind tails (Figure 2b), in which the apex is oriented in the

Figure 4. Various types of soils identified in Gusev crater: (a) Pancam image of bright dust coating the small rock named "Route 66" taken on sol 100 (L_s 19.4°) in zone 2; the dark circular patterns show where the RAT brush has removed the dust revealing the underlying dark rock, (b) MI image of soil consisting of a mono-layer of coarse (~1 mm) grains taken on sol 52 (L_s 355.3°) in zone 1, (c) MI of soil containing irregularly shaped lithic fragments as large as 6 mm across, taken on sol 46 (L_s 352.3°) in zone 1 within a small "hollow," (d) soil displaying fracture pattern (dark areas) suggestive of a cohesive crust where the rover wheel disturbed the soil and a small rock, imaged by Pancam on sol 90 (L_s 14.6°) in zone 1, and (e) Pancam view taken on sol 130 (L_s 33.8°) in zone 2, where the rover tracks revealed dark soil.

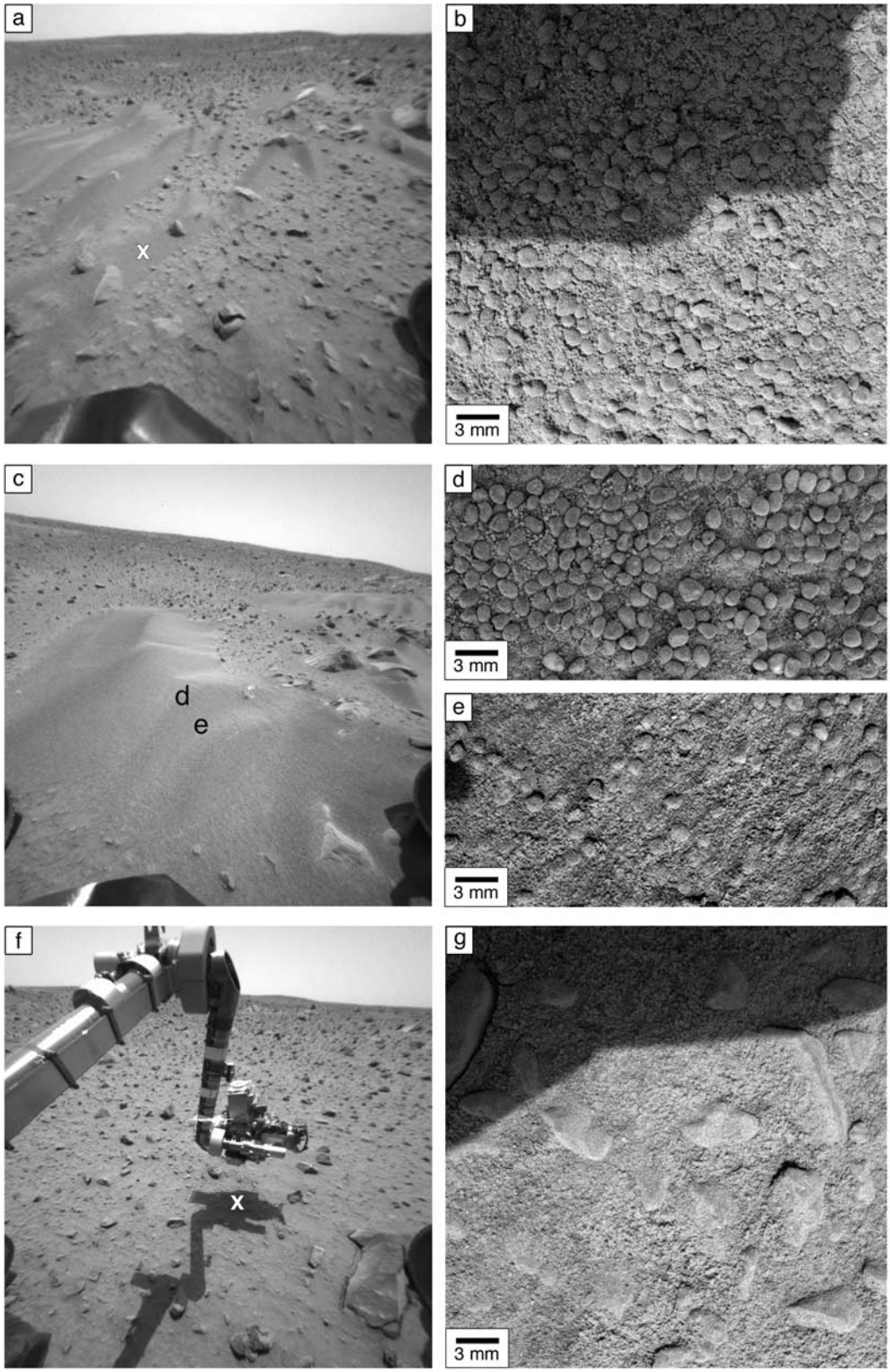

Figure 5. Soil characteristics for (a) the bed form named ''Drifter'' viewed in this Hazcam image in zone 1 (looking northeast) and the surface deposits seen in an MI image, (b) partly in shadow in upper left, (c) Hazcam image toward the northeast of the bed form ''Arena'' and the location of (d) the MI image taken on the crest of ''Arena'' and (e) the location of the MI image taken on the trough of ''Arena,'' (f) Hazcam view of ''Ramp Flats'' and the location (cross) of the (g) MI image of the soils. Sun is from lower right in MI images.

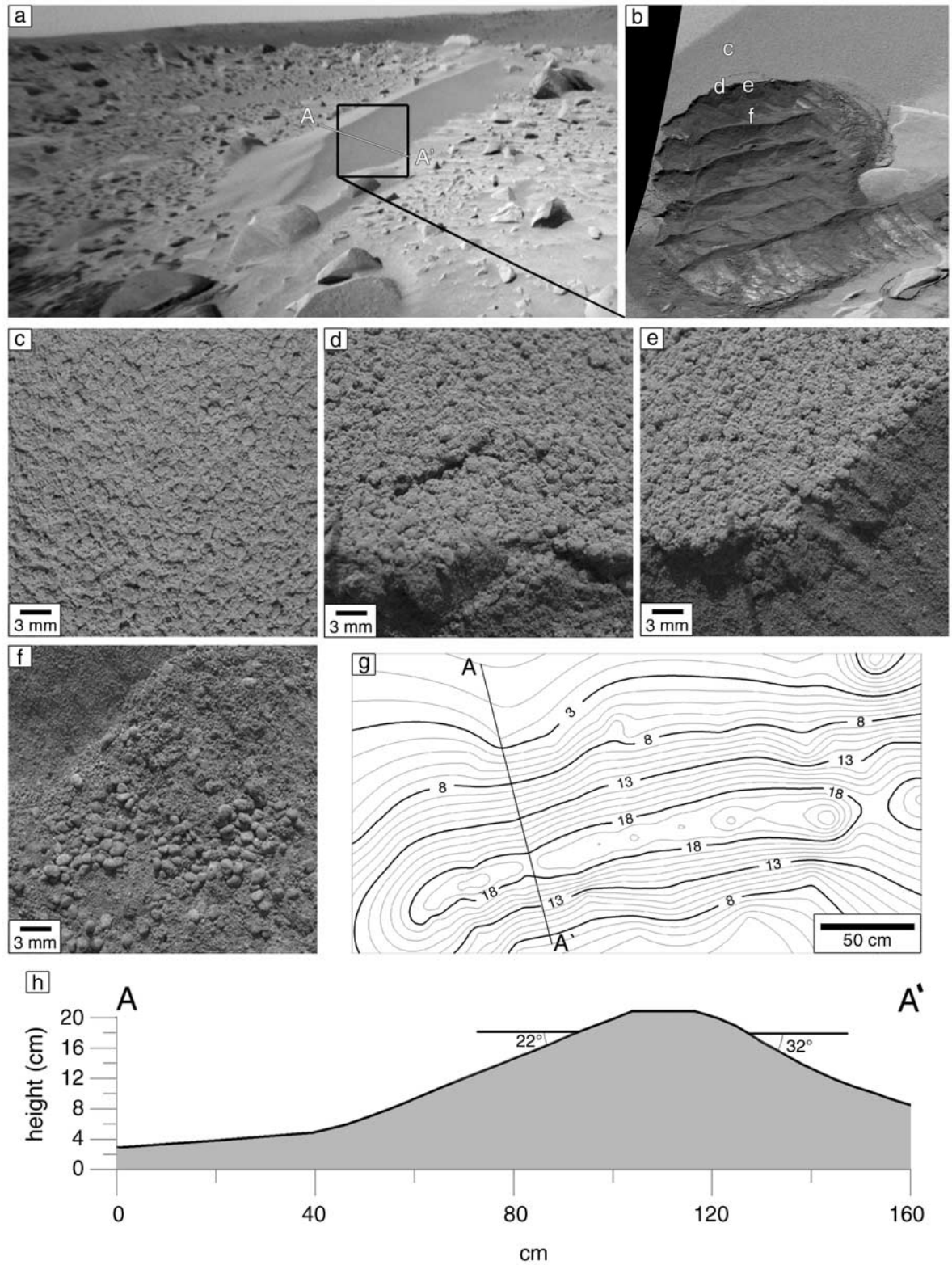

Figure 6. (a) Hazcam image of the bed form "Serpent" (zone 2), showing cross section (A–A), and outline of the frame shown in Figure 6b. (b) Rover wheel operations "cut" into the side of the bed form, as imaged by the Pancam. Boundary of the (c) disturbed and (d) undisturbed (e) bed form and (f) the debris in the disturbed part. (g) Topographic map of the bed form constructed from the Navcam stereo images. (h) Cross section taken along A–A (see Figures 9d–9g for location) showing the inferred "slip face" at 32° on the south-southeast side; the near-symmetry of the bed form in cross section suggests the presence of reversing winds.

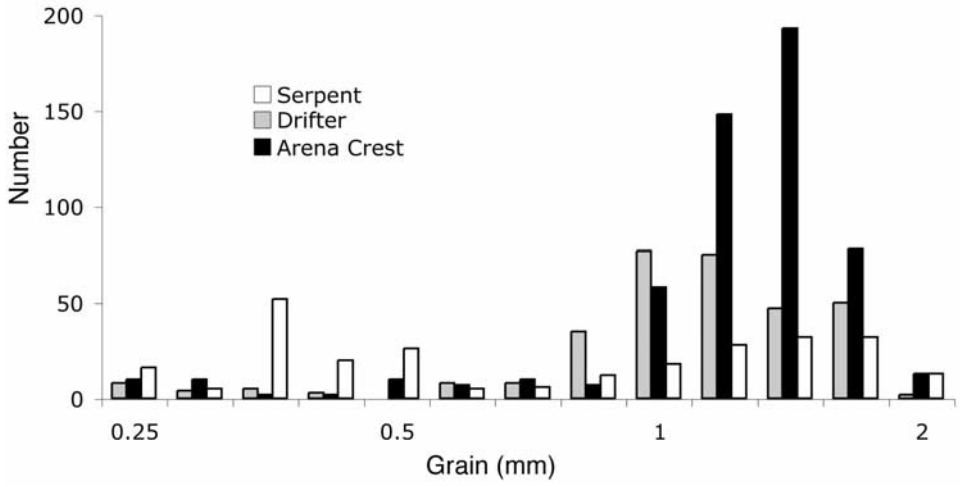

Figure 7. Grain size distributions determined from MI images for the bed forms "Serpent," "Drifter," and the crest of "Arena"; grain size shown on log scale.

inferred downwind direction (Figure 11). Wind tails could be primary depositional features, similar to coppice dunes that form on Earth around obstacles such as bushes, which can form a "dead" or "shadow" zone for wind. Alternatively, they could be erosional remnants of previously more extensive deposits [*Greeley et al.*, 2002]. In either case, they represent a zone in the local wind regime that is protected from wind erosion by the rock or obstacle with which they are associated. Wind tails in Gusev range in length from <10 to ~100 cm long and are most numerous in zone 3. As shown in Figure 10, their common orientation along the traverse indicates formative winds from the north-northwest, although in zone 2 the orientations suggest a bimodal distribution of formative winds from the southeast. In zones 4 and 5, the wind tails suggest a broader range of formative wind directions most likely resulting from the topographic influence of the Columbia Hills.

[31] Figure 12 shows two sets of bed forms in zone 1 near the landing site. The larger bed form (lower left corner) appears to be superposed on the wind tails, with the contact being relatively sharply defined. The orientation of the bed forms and the wind tails suggests winds from the right (southeast) in the image. This is in contrast to the formative winds from the asymmetric bed forms which suggest that the bed forms passed over the wind tails, and that the materials comprising the wind tail were sufficiently cohesive to be undisturbed. If this is correct, then the grains might be indurated, perhaps by cementation, suggesting that they are immobile and relatively older. Alternatively, the small wind tails could be erosional remnants left by the passage of the larger bed forms.

3.2. Wind Erosional Features

3.2.1. Ventifacts

[32] Wind eroded rocks (ventifacts) occur in two forms in Gusev, as planar surfaces called facets (Figures 3d and 13c–13d) and as grooves (Figures 2d, 3e, 13a–13b, and 13e–13f). As reviewed by *Greeley and Iversen* [1985], ventifacts form primarily by abrasion of windblown particles. Facets form orthogonal to the prevailing wind direction(s) responsible for "driving" the particles. Multiple facets can occur, and the terms einkanter, zweikanter, and dreikanter (from the German for one-, two-, or three-edged rocks) are applied to one, two, or three facets on any given rock (reviewed by *Livingstone and Warren* [1996]). Rocks with more than one facet can result from multiple wind directions, shifting and overturning of a rock to present a new surface to abrasion, or to complicated patterns of air flow and abrasion. Facets in Gusev are as large as 1.2 m across. Most of the faceted rocks occur in zones 1, 2, and 5, with only 7 occurrences in zones 3 and 4 combined. Orientations of the facets (Figure 10) in zones 1–3 are somewhat scattered, but tend to indicate formative winds from the north-northwest, with the suggestion of a secondary formative wind from the southeast for zone 2. Formative winds for the facets in zone 5 are relatively uniform from the northwest. Grooves constitute more definitive ventifact features than the inferred wind-eroded facets. As shown in Figures 13b and 13f, grooves include wide, scalloped hollows as large as 20 cm across on rocks, to narrow depressions. Following the convention used by *Bridges et al.* [1999] for similar features seen at the Mars Pathfinder site, the orientations of the ventifact grooves in Gusev suggest formative winds from the northwest for zones 1–3; as with the faceted rocks, there are very few rocks that exhibit grooves in zone 4. Grooves in zone 5 suggest formative winds from the southwest which is attributed to the topographical influence of the Columbia Hills. A few rocks show ventifact grooves that originate at a common level a few cm above the surface (Figure 14). This suggests that the rock contained a horizon that facilitated groove formation, such as a fracture, or that the rock was partly buried and shielded from abrasion. If this latter were the case, it would suggest that the surface has been "lowered" by 8 cm, perhaps by deflation of the surrounding soils.

3.2.2. Perched Rocks

[33] In several places along the traverse, rocks are seen that are "perched" on the tops of larger rocks (Figures 3f and 15). As discussed previously [*Greeley et al.*, 2004], these are thought to represent remnants of mantling debris that covered the area burying the underlying rocks. Through subsequent deflation, the fine materials were removed, and

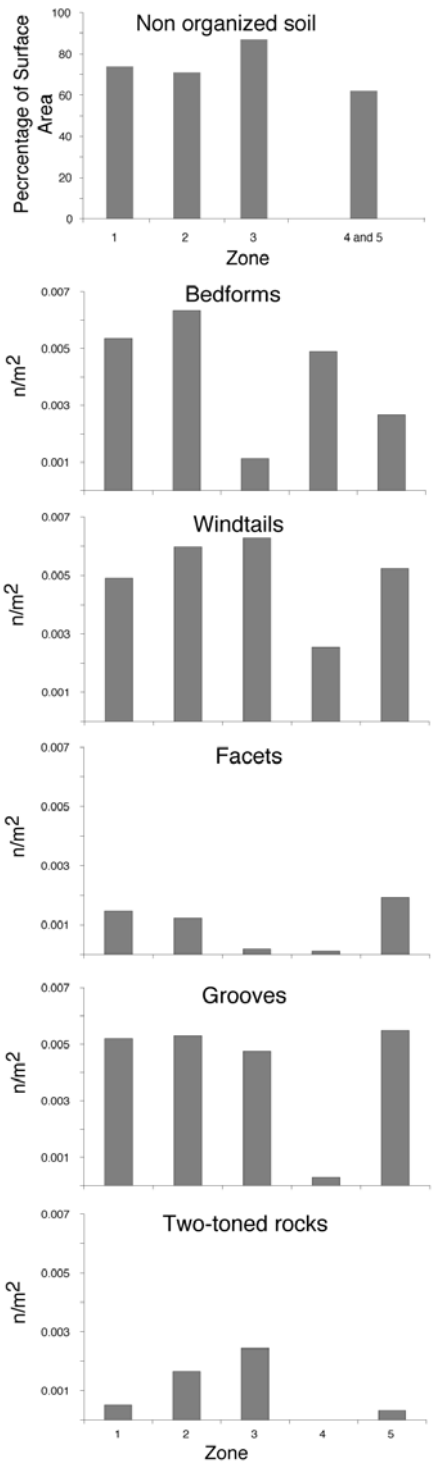

Figure 8. Histograms of the frequencies of aeolian features, normalized to numbers per unit area, for the five zones along the traverse of Spirit.

the larger materials, including small rocks, were ''lowered'' to the evolving surface. Some of these rocks are thought to have then been left ''perched'' on other rocks. Alternatively, the ''perched'' rocks could simply represent in situ weathering along a plane of weakness. They might also be ejecta from impact events, with the by chance emplacement on the tops of other rocks. The ''perched'' rocks are as high as 16 cm above the surrounding surface; if they represent deflation, then these values reflect the removal of material by those minimum amounts.

3.2.3. Two-Toned Rocks

[34] Many of the rocks observed on the surface throughout the traverse display a light-toned band at their base that is in contrast to the rest of the rock (Figure 2e). Similar features were observed at the Mars Pathfinder site where they were attributed to rocks that had been partly buried by soil, and then exposed by deflation [*Smith et al.*, 1997] or by temporary partial burial due to a passing aeolian bed form [*Greeley et al.*, 1999]. Similar explanations can be applied to the two-toned rocks in Gusev crater. We suggest that during partial burial, the lower part of the rock may have experienced precipitation of minerals on the rock where it was in contact with the soils, lightly cementing the observed fine soil in place. In situ measurements by Spirit (pre-RAT brush) were made on the light-toned parts of the rock, Mazatzal (Figure 13b) and were found to have chemistry with elevated amounts of sulfur and chlorine similar to the soils in Gusev, at the Mars Pathfinder site, and at the Viking Lander sites [*Gellert et al.*, 2004; *Morris et al.*, 2004]. Post-RAT analysis shows a lack of the elevated sulfur and chlorine, but yield compositions similar to the dark basaltic rocks in the area. Thus *Gellert et al.* [2004] suggested that the light-toned material was a coating that could be either a layer of dust or an alteration product. In either case, if saltating sands were abundant, one would expect the removal of the coating by sand impacts. Moreover, the grooves on Mazatzal (Figure 13b), which are considered to have been cut by sand abrasion, are light toned, suggesting that the coating was emplaced after the grooves were cut.

[35] If the two-toned rocks indicate widespread deflation, then they enable an estimate of the amount of deflation that has occurred on the surfaces surrounding the rocks. About 260 two-toned rocks were seen in sufficient detail to determine the height of the horizon. Heights range from <0.1 to 27 cm above the surface (Figure 16), with an average of 3 cm and giving an indication of the possible deflation. There is no trend in the heights of the horizon as a function of zone or location along the traverse. However, as noted by *Greeley et al.* [1999] at the Mars Pathfinder site, these heights do not necessarily mean that the entire surface on the floor of Gusev crater has been lowered by this amount, because the same values could result from the migration of a bed form over the rocks, partly or completely burying the rocks and leading to subsurface chemical weathering.

[36] Thus there is an inconsistency in the observations that remains unresolved. The occurrence of the perched rocks would tend to indicate a widespread mantle that has been removed; in this case, one would expect all of the rocks that were buried or partly buried should show the light coating. On the other hand, the observation that only some rocks have light-toned coatings suggests that the mantling was not contiguous, or of uniform thickness.

4. Features Seen From Orbit

[37] Numerous wind-related features are seen from orbit in the Spirit operations area. These include dune forms, dark

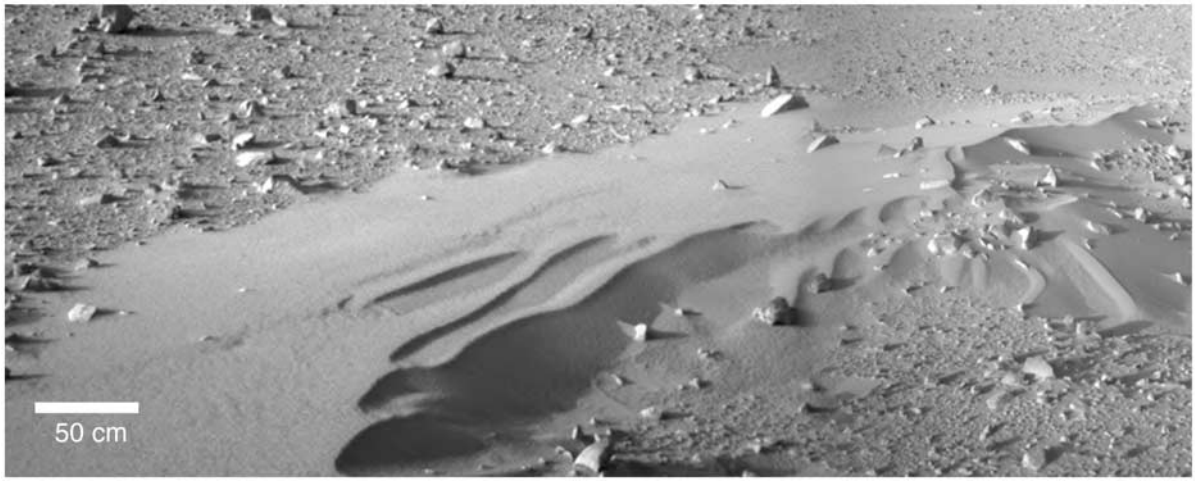

Figure 9. Mosaic of two Navcam images taken on sol 111 (L_s 24.8°) in zone 3 showing multiple bed forms that have partly merged to form a larger mass; the shadowed area in the middle foreground is inferred to be the slip face for the mass, which would imply formative winds from the upper left toward the lower right (toward the southeast).

wind streaks associated with topographical features, and dark linear streaks. Both types of wind streaks are albedo patterns that appear darker relative to the surrounding terrain (Figures 17d–17f). They are considered to represent local erosion, in which bright material, such as dust, is mobilized by the wind, exposing a relatively darker substrate. Dark wind streaks associated with craters and other topographic features, such as ridges, are clear indicators of formative wind directions (Figures 17d and 17e). As shown in Figures 18b and 18c, most of these appear to be from the northwest, especially at the CMS. Dark linear streaks are considered to be tracks left by the passage of dust devils [*Grant and Schultz*, 1987; *Malin and Edgett*, 2001]. In most cases, it is not possible to determine the initial and terminal points on the linear streaks (Figure 17f) that would indicate the wind direction, but it is assumed that the wind was approximately parallel to the general axis of the streak.

[38] Dune forms are small linear to curvilinear positive relief features and in Gusev they are found on the plains and on the floors of small craters. We note that similar small features are found in many regions of Mars, but there are insufficient data to determine if they are dunes, large ripples, or some other type of bed form. Nonetheless, they are considered to be accumulations of sand-size grains transported principally in saltation. As with bed forms, transverse dunes have crests that are orthogonal to the prevailing formative winds. Consequently, the azimuths of the dune crest axes (Figure 18a), represent winds from either the north-northwest or the south-southeast. Unfortunately, it is not possible to identify points, or "horns" (typical of barchan dunes) on the curvilinear dune forms that might be indicative of wind direction. However, when the dark wind streak orientations are taken into account, the formative winds are interpreted to be approximately from the north-northwest.

[39] THEMIS images taken over Gusev crater on 26 September 2003 (L_s 268°) before the landing of Spirit were compared with HRSC images taken 16 January 2004 (L_s 334°), shortly after the landing and about 2 weeks later on 1 February 2004 (L_s 343°) [*Greeley et al.*, 2005a, 2005b]. In general, all types of dark wind streaks tended to "fade" with time, apparently as a result of dust settling from the atmosphere. However, new dark features also developed in this interval. The orientations of the new dark wind streaks suggest formative winds from the northwest, consistent with the other features seen on the ground from orbit and with the wind directions inferred from features seen from Spirit.

5. Wind Regime

[40] The Athena payload has no provision for measuring winds. However, there are some direct and indirect means to interpret active winds during Spirit operations. These include observations of changes on and around the rover that are attributed to wind and comparisons with predictions from models of the atmosphere.

5.1. Observations

[41] The MER Rock Abrasion Tool (RAT) [*Gorevan et al.*, 2003] is used to brush or grind the surface of rocks. In the process, debris is ejected on radially symmetric trajectories, as determined by prelaunch laboratory tests. Deviations from a radially symmetric pattern can be attributed to factors such as the shape of the surface surrounding the RAT site, or by the presence of wind during the operation, which might carry the debris in a down-wind direction (Figures 19a–19c). Initial results from Spirit showed that RAT grinding on the rocks Humphrey (L_s 359°; 1100–1500 LST) and Adirondack (L_s 345.8°; 1220–1520 LST) were asymmetric, and were interpreted to result from winds from the northwest (Table 3) [*Greeley et al.*, 2004]. Subsequently, additional rocks were abraded using the RAT, providing seven asymmetric patterns and four symmetric patterns. On the assumption that the asymmetric patterns result from winds at the time of RAT operations, most of the inferred winds were from the northwest (Figure 19d). The exception is the pattern for the rock Wishstone, which suggests active winds from the west.

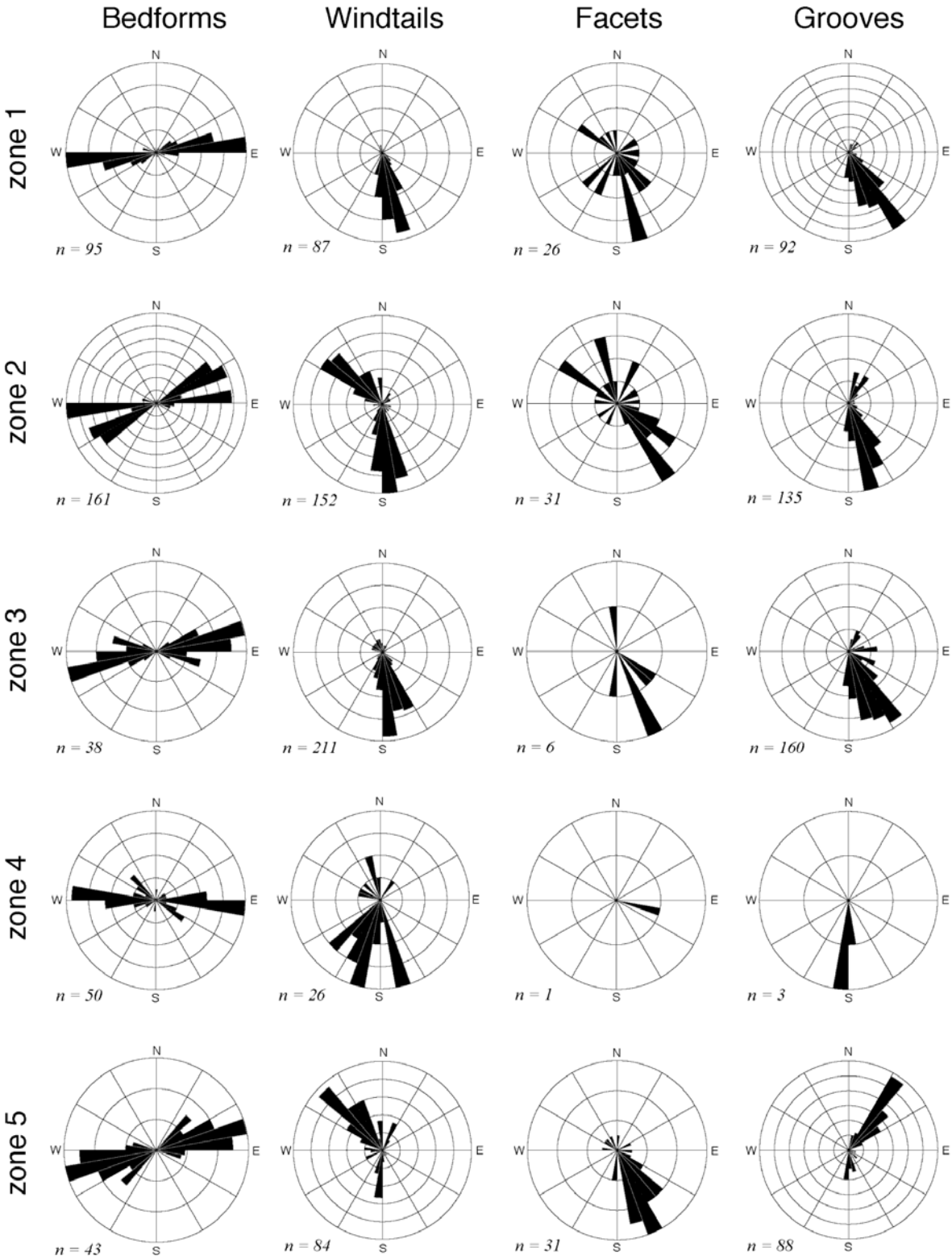

Figure 10. Rose diagrams showing the orientations of wind-related features by zone along Spirit's traverse to the Columbia Hills; *n* refers to the total samples in each diagram.

[42] For the most part, Spirit was seldom in one position for an extended time to monitor potential changes on the surface. However, during solar conjunction from 5 to 26 September 2004 (L_s 83.1° to 93.1°), the rover was in one position (or "stand down") for 20 sols on West Spur within the Columbia Hills. Images taken before and after this period showed slight changes in color and albedo on the surface that were attributed to movement of material

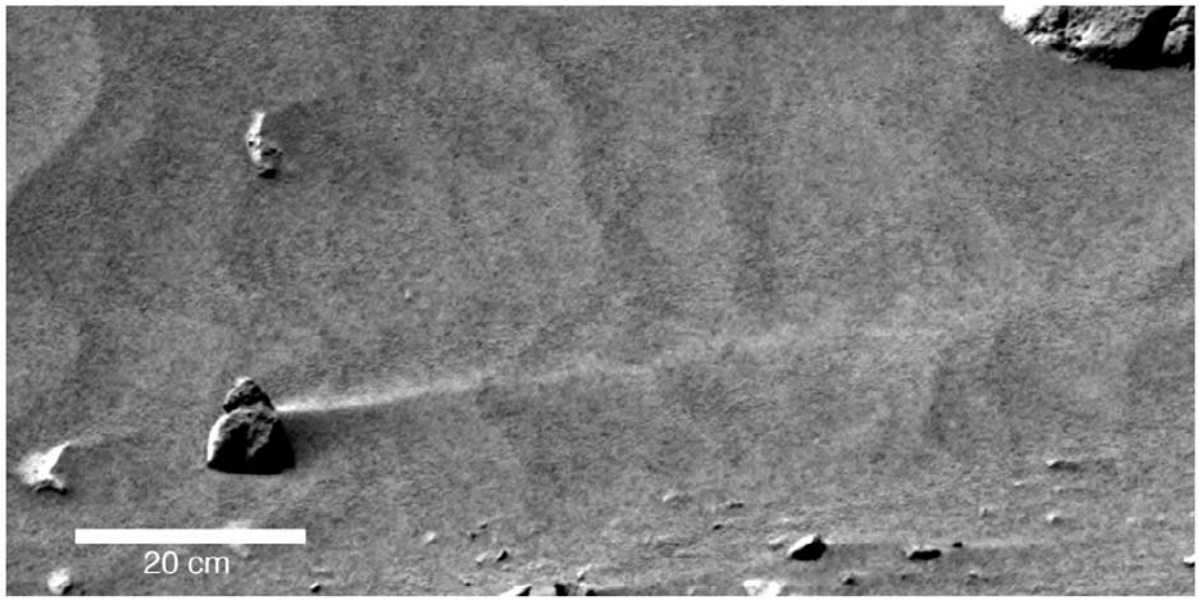

Figure 11. Pancam image of a wind tail formed in the lee of a small rock in zone 5.

[*Greeley et al.*, 2005b]. The location of the changes coincided with the surface beneath the body of the rover where winds would have been accelerated, as determined from wind tunnel simulations [*Neakrase et al.*, 2004]. In addition, MI images taken before and after the conjunction of an area in front of the rover showed individual sand grain movement of as much as 0.7 mm. These observations suggest that winds were of sufficient strength to move some particles

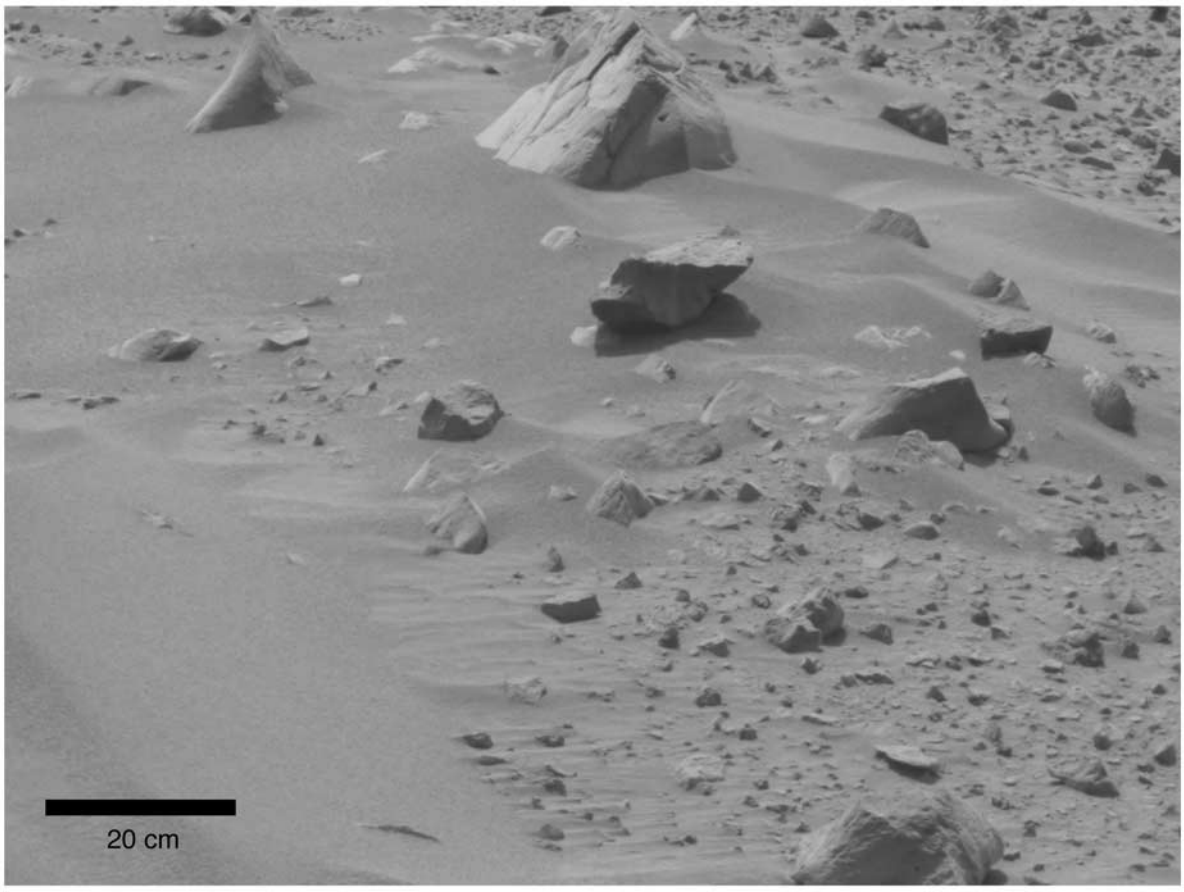

Figure 12. Pancam image of a bed form (lower left, with superposed scale bar) superposed on smaller features inferred to be wind tails.

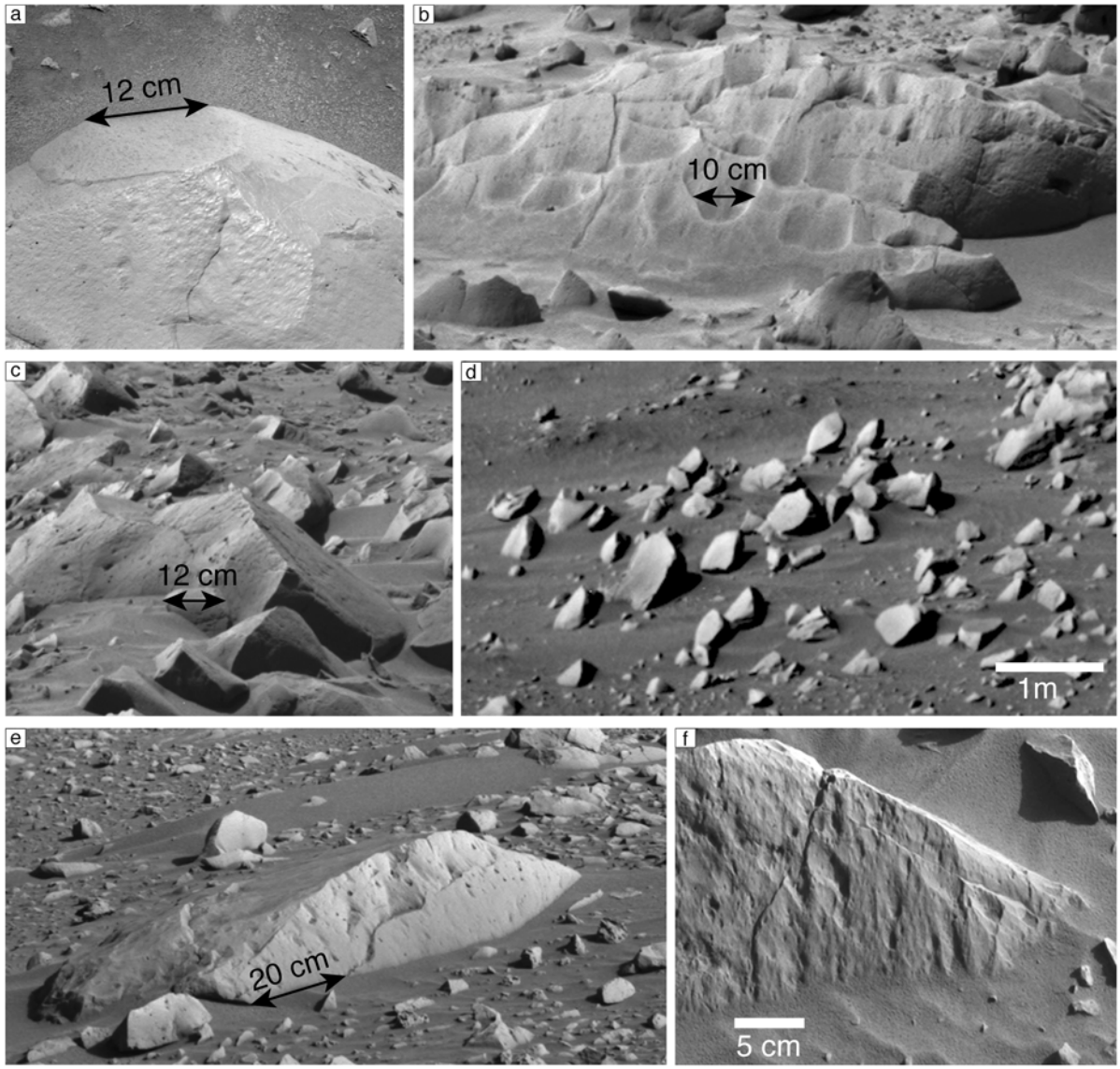

Figure 13. Wind-eroded rocks, or ventifacts: (a) the rock ''Adirondack'' showing a flat, smooth face, or facet, (b) the rock ''Mazatzal'' in zone 2 showing wind-eroded grooves, (c) small rocks showing facets imaged by Pancam in zone 2, (d) a field of rocks in zone 4 showing facets, (e) rock in zone 1 showing a facet with grooves, and (f) Pancam image showing small grooves.

slightly, and the locations and orientations of the movement suggest winds generally from the northwest.

[43] Beginning on about sol 417 (L_s 170.9°), various features were observed on the rover, which are attributable to active aeolian processes. Until this period, there was a steady decrease in output from the solar panels, which was attributed to dust settling from the atmosphere. On sol 420 (L_s 172.7°), the output increased markedly and is thought to have resulted from clearing the dust from the solar panel by wind, perhaps by one or more wind gusts or dust devils. In the same period, dust accumulated on parts of the deck where flow was obstructed, including a zone in the ''shadow'' of the Pancam calibration target. From the orientation of the rover and the dust deposit, the winds appear to have been from the southeast toward an azimuth of 310°. In addition, a marked ''blurring'' of the Hazcam images suggested that dust might have accumulated on the lenses initially on sol 417; subsequent images beginning on sol 420 suggest that the dust was removed.

[44] Beginning on sol 421 (L_s 173.2°) active dust devils (Figure 20) were observed on the floor of Gusev crater (Figure 1) in Hazcam, Navcam, and Pancam images from Spirit's perspective in the Columbia Hills. The dust devils are as large as 40 m in diameter (consistent with the widths of some of the dark linear wind streaks seen from orbit) and at least 158 m high. From the tilt (''leaning'' in the downwind direction) of the column, the inferred directions of motion were toward the south, north, and east; in one case, sequential images indicate the rate of motion across the plains was 2.5–3.8 m/s.

[45] In addition to active dust devils, there is also indication of active sand saltation in the Columbia Hills. MI

Figure 14. Rock "Terrace" imaged by Pancam in zone 2, showing the grooves that originate from a common horizon, which could represent either a zone of weakness, such as a fracture, or partial burial of the rock which shielded it from wind abrasion, and a rock that appears to be "perched."

images taken on sol 431 (L_s 178.9°) of the rover deck (Figure 21) show the accumulation of several hundred sand grains, some as large as 300 μm in diameter, which were not present on sol 350 (L_s 135.4°). Subsequent images on sol 505 (L_s 224.2°) show the accumulation of additional grains in the same area. We suggest that these sand grains were emplaced by saltation, which might have been "driven" by wind gusts.

5.2. Atmospheric Model Predictions

[46] Gusev crater is situated within two cells (7.5° by 9° each) of the MGCM. Model predictions for the fall season and early spring show prevailing wind directions from the south-southwest, with strongest winds occurring in the early winter (L_s 90°–135°). However, in the late spring and summer, winds nearly reverse with the prevailing directions from the north and northwest.

[47] As noted in section 3, the MGCM predictions are appropriate on global scales, reflecting the Hadley circulation, major topographic influences (such as the highland-lowland dichotomy), and tides. Circulation on the scale of Gusev crater cannot be resolved by the MGCM. MRAMS runs take into account the influence of topography on the scale of Gusev crater (using the 1/32° gridded MOLA data), although we note that the topography of the ~2 km by 5 km Columbia Hills complex has not been modeled. As shown in Figure 22, diurnal patterns within Gusev crater are much more important for comparisons with local surface features than the MGCM results. In all seasons, the general wind pattern during the night is down-slope flow from the high-standing areas (such as the crater rim) and flow from Ma'adim Vallis onto the floor of the crater. Analyses of the MRAMS results suggest that during the day (with solar heating) the flow is radial from the middle of the crater floor up slope over the crater walls. During the night, the stable thermal stratification results in more laminar (less turbulent) flow, whereas during afternoon heating the turbulence increases and the formation of local dust devils are likely, as was observed from Spirit (Figure 20).

[48] Four MRAMS simulations with a smallest nest grid spacing of 3.75 km were run, with the first run centered at the season of the Spirit landing (L_s 328°) and the others were spaced by 90° of L_s (L_s 238°, 148°, and 58°) to assess atmospheric circulation for each cardinal season for 20 minute intervals during a sol. We note that the simulations are incapable of resolving any structure along the ~2.5 km rover traverse, because the model grid spacing is too large (i.e., the entire Spirit traverse fits within a single grid cell). Winds associated with the highest surface shear stress blow toward the southeast in spring and summer (~150°–155° azimuth) with the strongest winds in the afternoon. These winds from the northwest result from the combined effects of topography at different scales: (1) Gusev crater's location on the margin of the southern highlands, in which regional daytime upslope winds are driven from the northwest, (2) the low northern crater rim, which allows the regional winds to flow into the crater, and (3) the relative steepness and height of the southeastern rim, which accelerates daytime flow that enters the crater from the north. These daytime winds (Figures 22a and 22b) are present at all seasons, but are modulated by seasonal changes and associated heating. Nighttime to early morning winds (Figures 22c and 22d) involve reversed flow from high-standing areas into the crater, with increased air flow channeled into Gusev from Ma'adim Vallis. Nocturnal winds tend to be strongest during the autumn and winter seasons and are from the south-southeast. The strongest daytime winds are in the summer and are from the north-northwest. In all seasons there is large variability in diurnal winds and a relative lack of strong winds to saltate sand at the CMS. This lack, however, does not preclude the possibility of local gusts and dust devils that could initiate particle movement as suggested in Figure

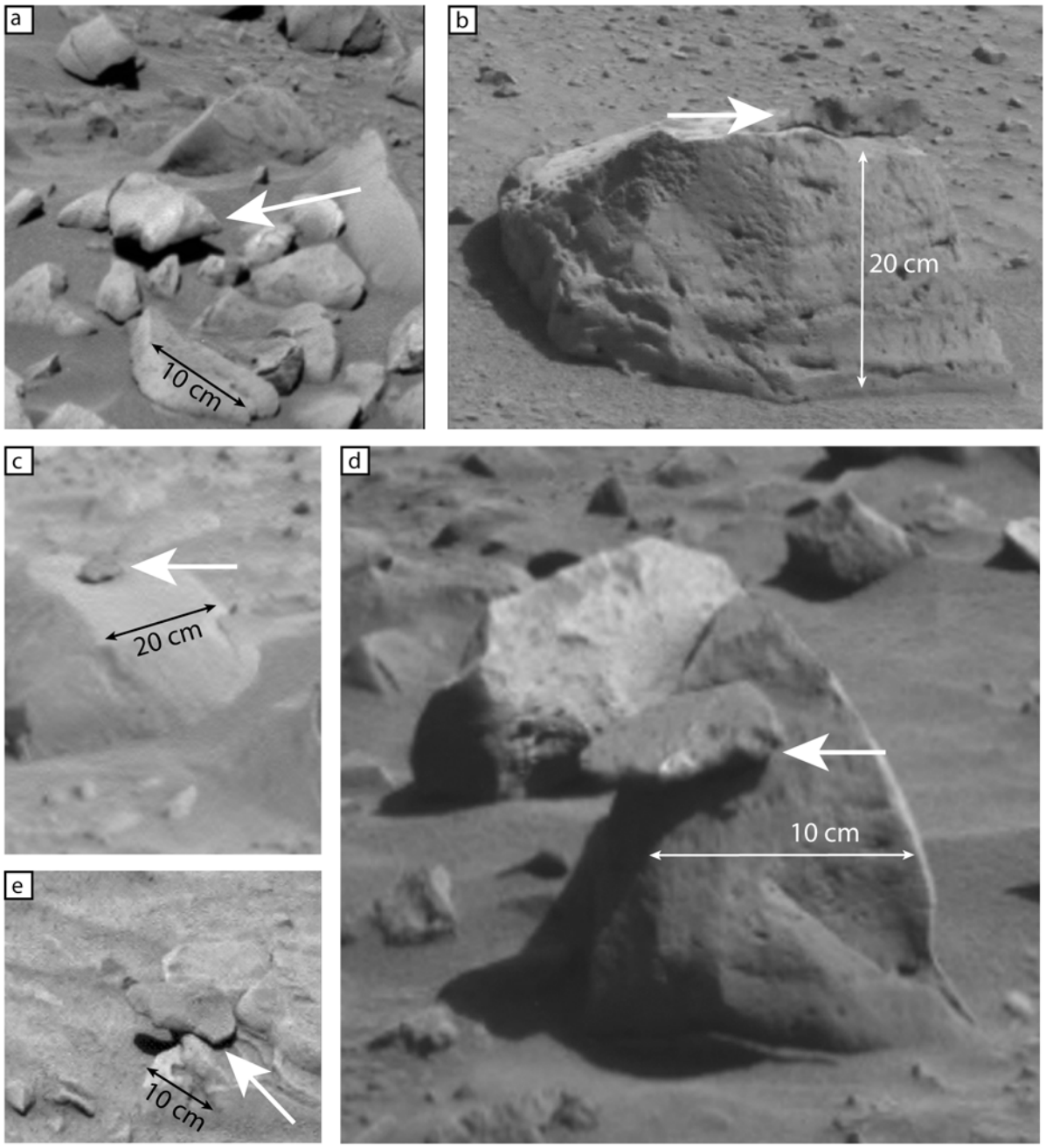

Figure 15. Various "perched" rocks (indicated by arrows): (a) Pancam image of rock in zone 2, (b) Pancam image of the rock "Gepetto" in zone 1, (c) Navcam image of rock in zone 2, (d) Pancam image of rock in zone 2, and (e) Pancam image of rock in zone 2. Perched rocks are thought to represent deflation, or lowering of the surface by removal of material by the wind, leaving some rock in "balanced" positions supported by one or more rocks.

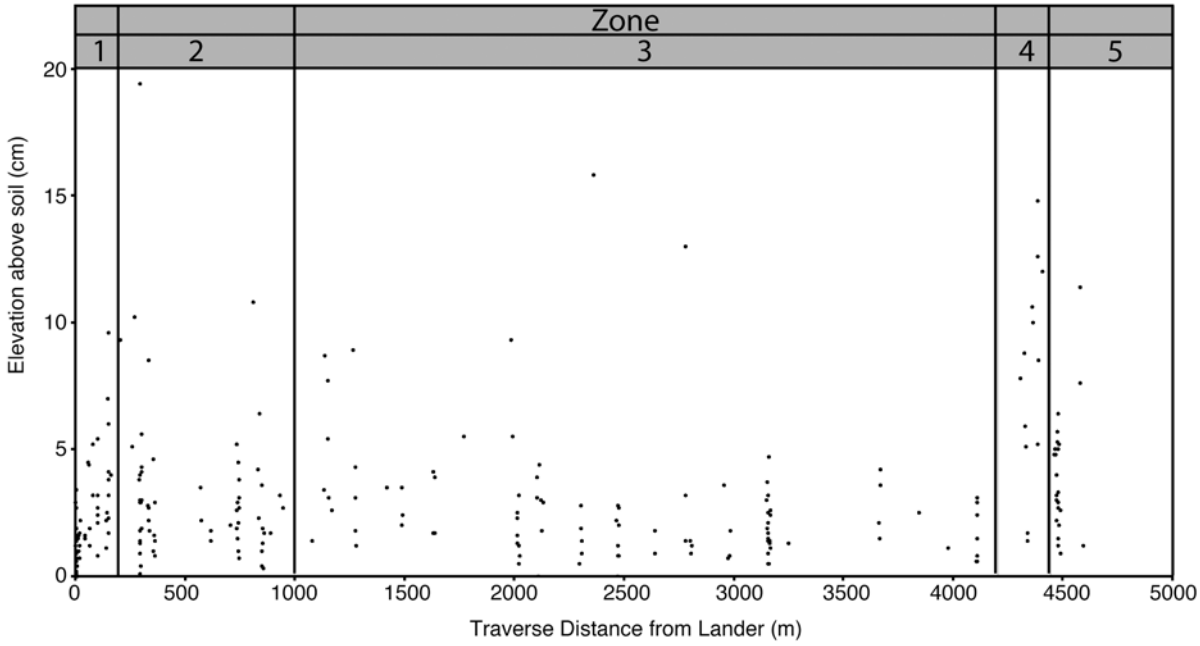

Figure 16. Height above the surface to the boundary between the lower light-toned part and the upper dark-toned part of "two-toned" rocks as a function of zone along Spirit's traverse.

21. Such winds would be too small to be resolved in the MRAMS grid used here.

6. Discussion and Conclusions

[49] Aeolian activity requires a supply of loose particles and sufficient winds to move them. Both sand and dust are present in Gusev crater, and observations from Spirit show that dust and possibly sands are currently active in some areas. Active dust devils on the floor of Gusev were observed in images taken from about noon to 1500 LST, when heating of the surface is expected to generate unstable conditions. Sand-size grains were also observed to move subcentimeter distances during the solar conjunction, although it is not clear that any grains were in saltation. Most of the bed forms and soil patches that contain sand appear to have intermixed dust, suggesting infiltration into sands. Thus it would appear that these sands are not currently experiencing active saltation because such activity should "purge" the finer grained dust from the deposit, setting it into suspension and removal from the bed form. Furthermore, an indurated armor of coarser grains is found on several of the observed bed forms. From the above observations and assumptions, we conclude that most of the sands along the traverse are inactive, although the sand grains on the rover deck that appeared on about sol 431 (L_s 178.9°) could indicate local saltation in the Columbia Hills.

[50] Small particles amenable for wind transport are produced by a wide variety of processes, including impact cratering, volcanism, and weathering of rocks. Salt weathering is a particularly effective mechanism for generating fine grains in terrestrial deserts [*Goudie et al.*, 1979]. In this process, salts in solution enter microcracks and crystallize, exerting forces sufficient to break the rocks and larger grains into smaller fragments, particularly dust. Given the possible salts detected from Spirit on rocks and in the soils [*Gellert et al.*, 2006; *Ming et al.*, 2006; *Morris et al.*, 2006], salt weathering could be an important mechanism for the generation of dust on Mars and within Gusev crater. The uniformity of dust compositions at the Viking lander, Mars Pathfinder, Opportunity-Meridiani site, and Spirit-Gusev sites suggest that Martian dust becomes globally "homogenized" after it is generated from various local sources. This is a reasonable assumption because dust can be carried to high altitudes in suspension where it is mixed and transported long distances.

[51] The numerous bed forms, such as ripples, signal the presence of sand-size grains that were moved in saltation. Sand-size particles can occur as holocrystalline grains or as aggregates (small clods) of dust held together, perhaps by salt cementation. MiniTES data argue for sand-sized basalt grains to produce the signatures seen. Although some particles imaged by the MI could be aggregates, the numerous ventifacts indicate that the grains are holocrystalline because laboratory experiments under Martian conditions show that aggregates cannot abrade rocks [*Greeley et al.*, 1982]. Sands and granules could be derived locally, or they could have been generated elsewhere and transported into Gusev crater by wind, water or as ejecta from impacts. Many of the Spirit images show granules and coarser clasts at the bases of rocks where they form apparent "lag" deposits, and the spectra of the particles appear similar to those of the rocks. This suggests that some rocks have been weathered in situ and "shed" debris that collects around the rocks. Acceleration of winds and turbulence around the rocks could remove the fine sands, leaving the coarser grains behind as a lag deposit.

[52] In order to evaluate the potential transport distance of sands in saltation, laboratory simulations were run under Martian conditions to determine the number of impacts that

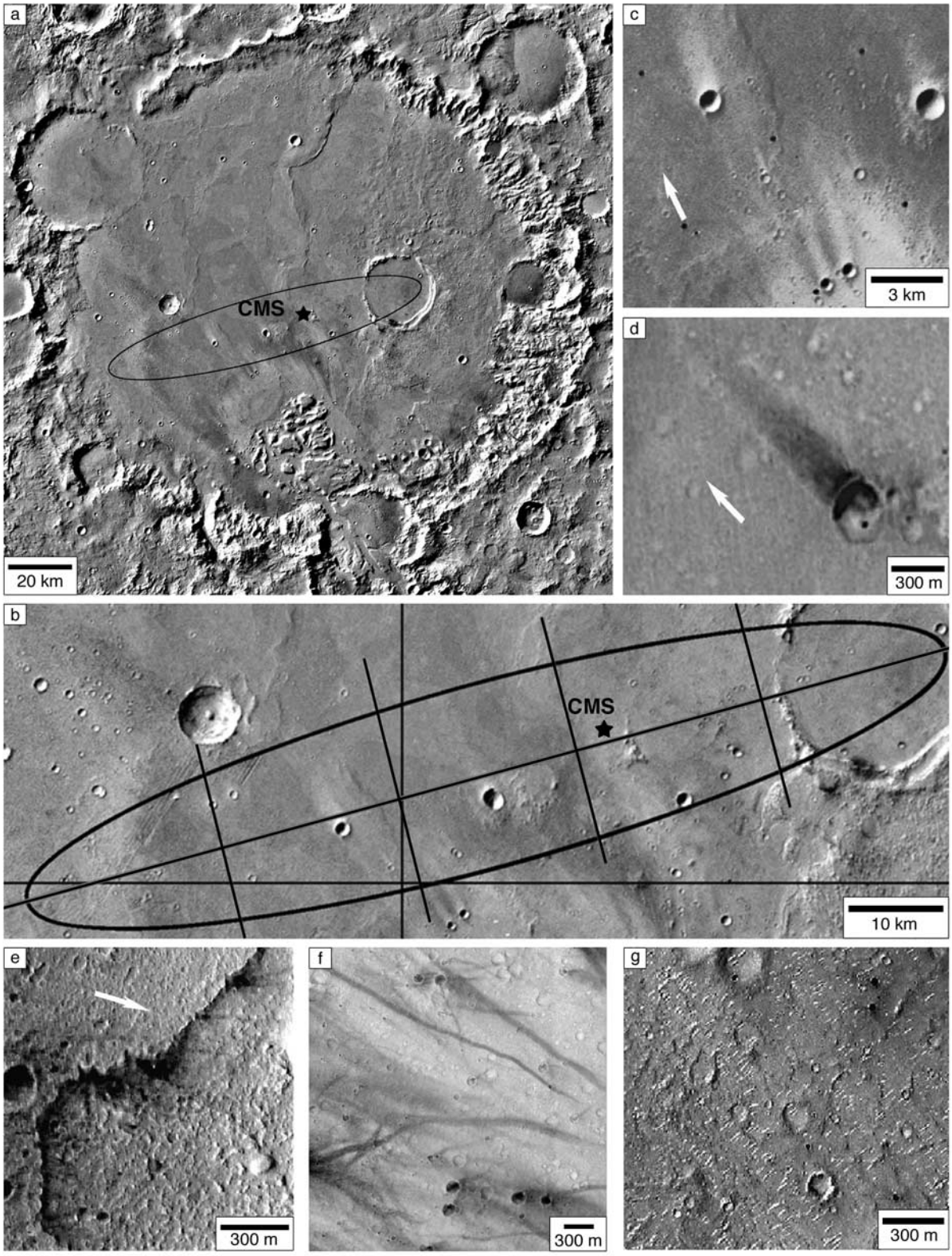

Figure 17. Wind-related features seen from orbit over Gusev crater: (a) location of the landing ellipse in Gusev crater and the location of the Columbia Memorial Station (CMS), (b) landing site ellipse showing the 10 ''cells'' within which wind-related features were analyzed, (c) bright wind streaks, (d) dark wind streaks, (e) dark wind streaks associated with a small ridge, (f) dark linear wind streaks inferred to be the tracks left by the passage of dust devils, and (g) small, bright ridges inferred to be bed forms.

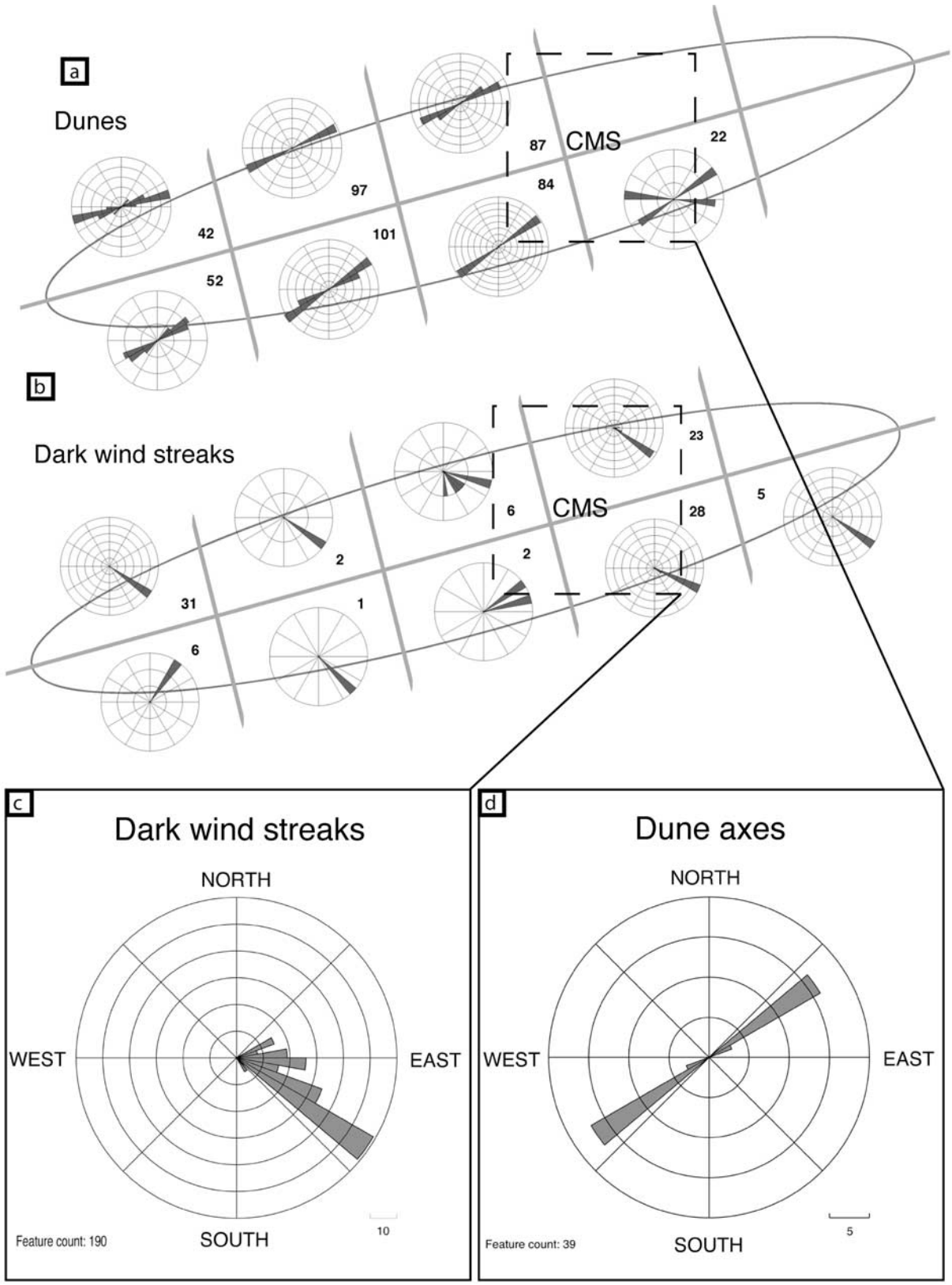

Figure 18. Rose diagrams of (a) dunes and (b) dark wind streaks within each cell in the landing ellipse. (c) Dark wind streaks and (d) dune axes for the dashed square cell centered on the Columbia Memorial Station (CMS).

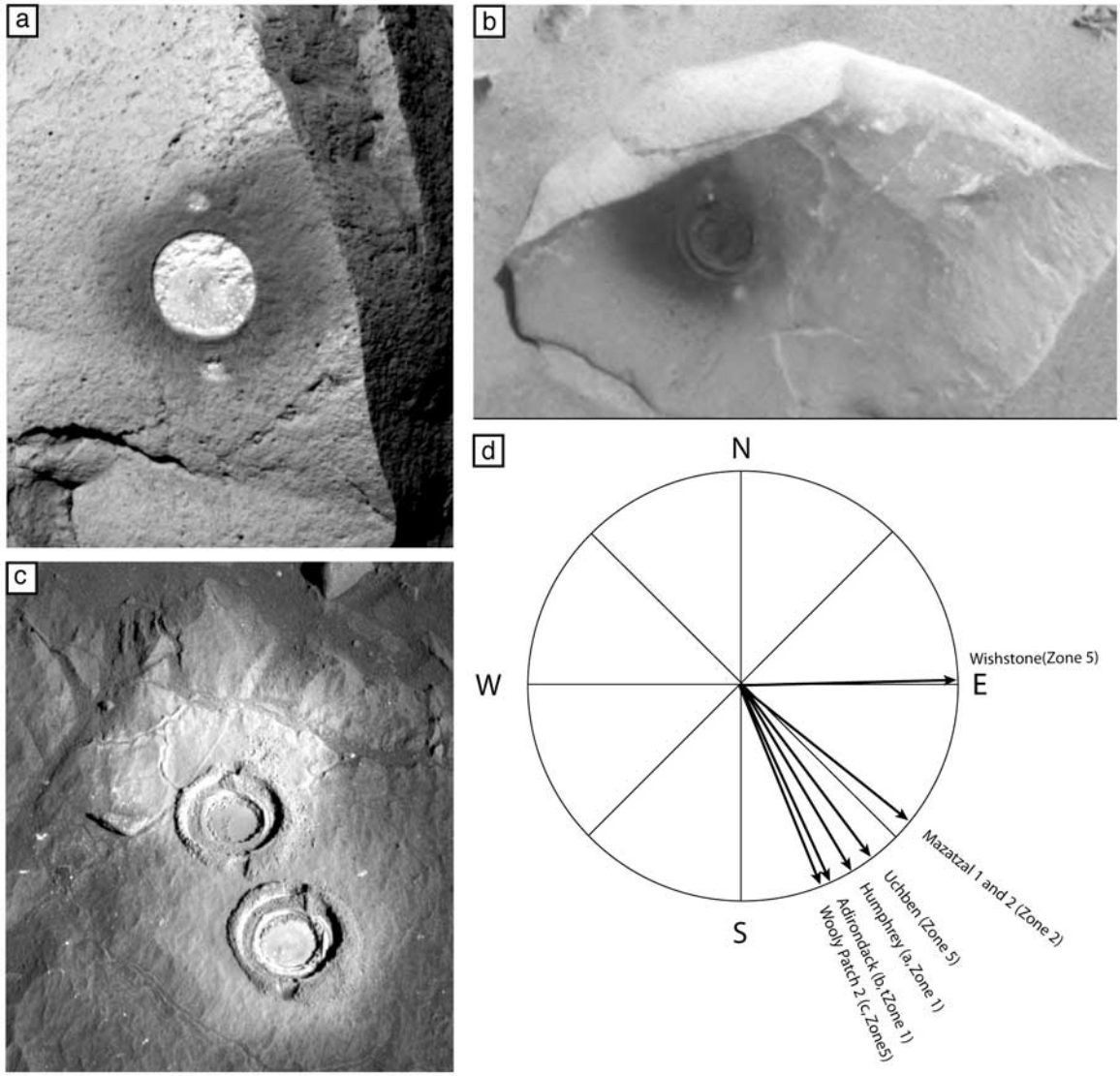

Figure 19. Wind directions inferred from the patterns of cuttings from the RAT, showing the rock (a) "Humphrey," (b) "Adirondack," and (c) "Wooly Patch 1 and 2," along with (d) the azimuths of these and other patterns.

grains would survive before being comminuted into dust-size particles that would be removed by suspension (i.e., no longer transported in saltation to develop bed forms). Results show that lithic and holocrystalline sand grains can survive sustained saltation impacts, enabling transport distances of 100s of km before being worn down into dust sizes [*Greeley and Kraft*, 2001]. Thus with the evidence for holocrystalline grains suggested by the presence of the ventifacts, it is possible that at least some sands that originated outside Gusev could have been transported into the crater by wind. Sustained transport is also suggested by the MI images that show well-rounded sand grains and granules.

[53] Comparisons of the frequencies and orientations of wind-related features along Spirit's traverse give insight into the aeolian regime and surface processes in the area. Zone 3, the long traverse from Bonneville crater to the base of the Columbia Hills, has the maximum frequency of "perched"

Table 3. Wind Directions Inferred From RAT Patterns

Zone	Rock Feature Name	Sol (Spirit)	L_s, deg	Operation Time, LST[a]	Inferred Wind Direction,[b] deg
1	Adirondack	34	345.8	1220–1520	157
	Humphrey	59	359.0	1100–1500	149
2	Mazatzal 1	81	10.1	1100–1440	130
	Mazatzal 2	83	11.1	1140–1500	130
4	Pot of Gold	169	51.6	1130–1315	none
5	Wooly Patch 1	195	63.4	1345–1530	none
	Wooly Patch 2	198	64.8	1320–1530	159
	Clovis	216	72.8	1250–1520	none
	Ebenezer	231	79.5	1220–1400	none
	Uchben	285	104.1	1320–1445	143
	Wishstone	334	127.4	1225–1340	88

[a]LST, local solar time.
[b]Azimuth toward which wind blew.

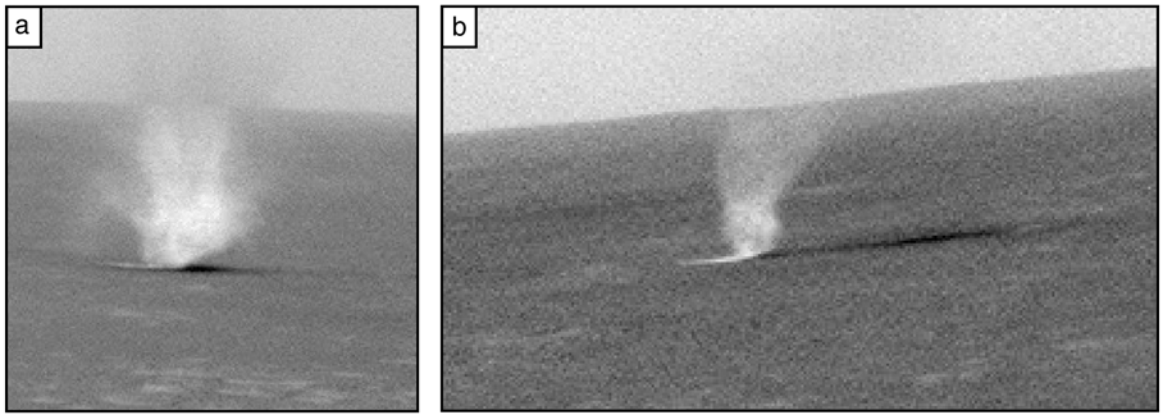

Figure 20. Active dust devils on the floor of Gusev crater viewed from the Columbia Hills: (a) Navcam image on sol 496 (L_s 218.4°) of a dust devil about 45 m in diameter and (b) Navcam image taken on sol 489 (L_s 213.9°) of a dust devil 23 m in diameter; sequential images suggest apparent movement of 5.0–6.0 m/s across the floor.

rocks and wind tails, and the maximum extent of soil patches that are not organized into bed forms. We interpret the ''perched'' rocks to represent net deflation, or lowering, of the surface. Similarly, the soil patches could be the remains of deposits that are stabilized, perhaps by cementation, or material that has not yet been removed. If these interpretations are correct, then this area appears to have experienced deflation of up to ~27 cm (at least locally), the maximum height to the boundary of the light-toned parts of two-toned rocks and the heights of the ''perched'' rocks.

[54] The orientations of most of the wind-related features seen from orbit and the ground suggest primary winds from the north-northwest blowing to the south-southeast, and a secondary wind from the southeast. The north-northwest direction correlates well with the predictions for strong afternoon winds, particularly in the summer and spring. These winds are attributed to the influence of topography and afternoon heating which result in turbulent flow up slope. However, the bed forms, such as the ripples, tend to be symmetric, which suggests reverse flow, consistent with nighttime winds predicted to be down slope from the crater rim onto the floor of the crater.

[55] The orientations and frequencies of aeolian features in the West Spur region of the Columbia Hills (zone 5) and the transition from the plains to the Hills (zone 4) appear somewhat anomalous in comparison to the other zones. For example, the ventifact groove orientations suggest formative winds from the south-southwest, orthogonal to the flow trends of resulting features seen elsewhere, which does not correlate with MRAMS predictions for any season or time of day. We suggest that local topography (not modeled by MRAMS) strongly influences both the direction and magnitude of the winds responsible for these aeolian features, as is commonly observed on Earth [e.g., *Greeley et al.*, 2002; *Bridges et al.*, 2004]. For example, winds moving up slope are commonly accelerated, at least initially, by flow compression, leading to increased abrasion and formation of ventifacts [*Bridges et al.*, 2004].

[56] The orientations of the wind related features observed by Spirit are much more consistent with the wind directions predicted by the atmospheric model than was observed at the Mars Pathfinder (MPF) site. At MPF, two prevailing winds were inferred [*Greeley et al.*, 2000], one from the northeast that correlates with atmposheric model predictions and a second wind from the east southeast that is not predicted for any current wind regime. The second wind pattern was suggested by the orientation of ventifacts seen on the surface and wind-eroded rims of small craters seen from orbit, and was attributed to a paleowind regime. No such pattern has been detected in Gusev crater in this study, but it must be noted that wind patterns in Gusev appear to be strongly controlled by local topography.

[57] In conclusion, aeolian processes involving both sand and dust are currently active in some parts of Gusev crater. It is likely that such processes have taken place throughout the history of Mars, so long as small particles and winds have been present. Although there are uncertainties in the detailed ages of the surfaces over which Spirit traversed, much of the floor of Gusev crater appears to be surfaced with basaltic bedrock emplaced some 3.5 Gyr ago, which would place an upper boundary on the age of the surficial deposits, including the aeolian features on the plains. The Columbia Hills, however, are thought to be older than the plains. Moreover, the rocks appear to be more weathered and are much softer than the plains basalts [*Arvidson et al.*, 2006; C. Schröder et al., manuscript in preparation, 2006] which would make them more susceptible to abrasion by windblown particles, and could lead to contributions of particles for wind transport.

[58] Several key questions remain to be resolved with regard to aeolian processes in Gusev crater.

[59] 1. Dust devils are clearly frequent at certain times of the year. What is their contribution to the total mass of dust injected into the atmosphere in comparison to local and regional dust storms raised by non-dust-devil processes?

[60] 2. Although there are indications that sand is active in some areas, what portion of the sand deposits experience saltation annually?

[61] 3. Do the light toned rocks and the ''perched rocks'' represent a widespread mantle that has been removed, presumably by wind deflation, or are they the result of the passage of local bed forms?

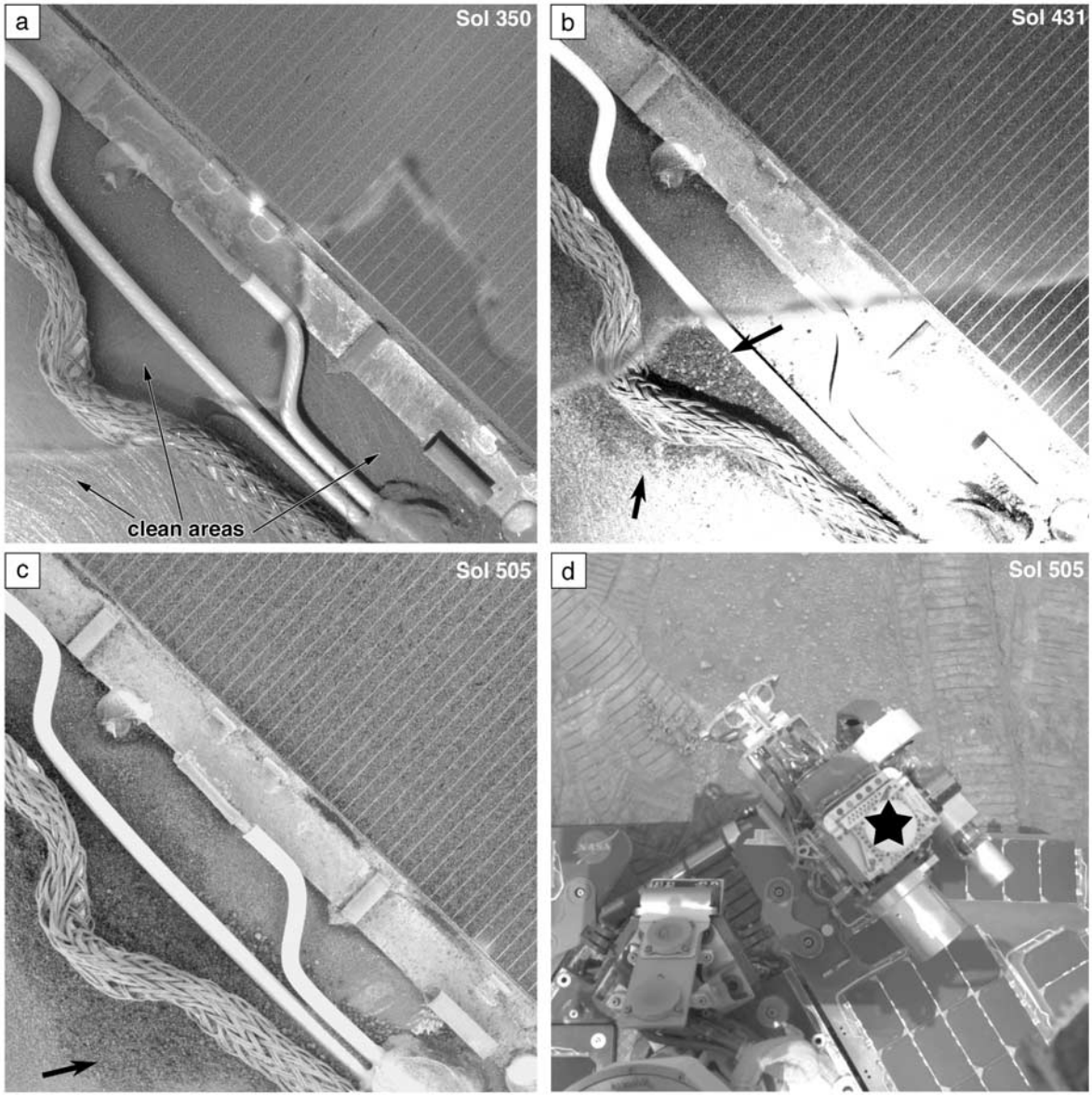

Figure 21. Part of the Spirit rover deck images by the MI (a) on sol 350 (L_s 135.4°), showing a ''clean'' surface, (b) on sol 431 (L_s 178.9°), showing accumulation of grains (arrow), and (c) on sol 505 (L_s 224.2°), showing additional accumulation of grains. (d) Navcam image showing context of the MI images, which were taken below the part of the payload marked with the star.

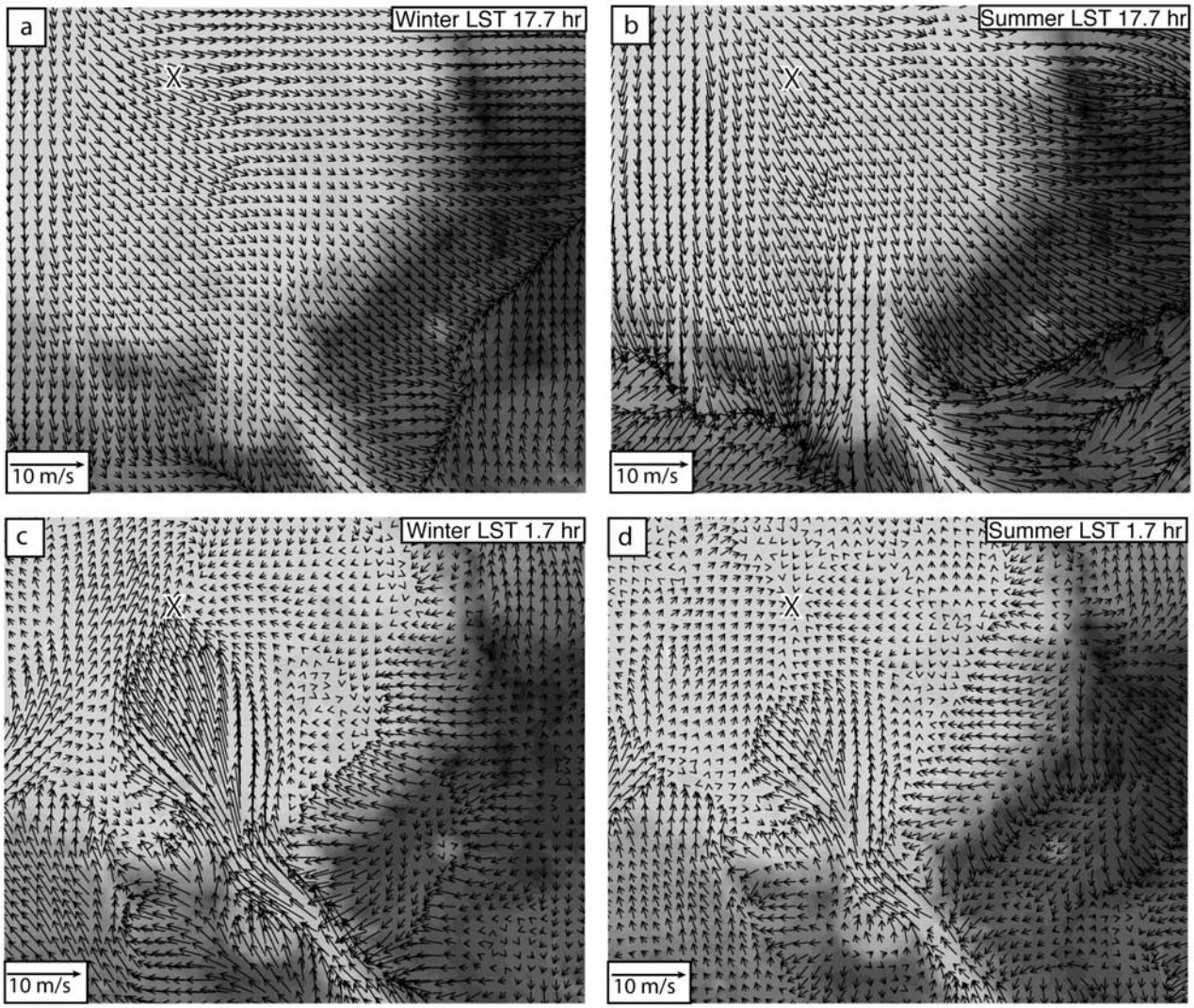

Figure 22. Winds predicted by MRAMS for the southeastern part of Gusev crater for late afternoon in the southern hemisphere (a) winter and (b) summer and for nighttime in (c) winter and (d) summer. Vectors represent azimuths toward which the winds blow, modeled at a height of 2 m above the surface. The cross marks the location of the Spirit landing and operations area. Wind vectors are superposed on MOLA topography, in which dark grey represents terrain at or higher than 1400 m above datum, and white (crater floor) is an elevation of −1900 m (below datum). This relief of 3.3 km generates substantial slope winds.

Table A1. Image Identifications for Figures

Figure	Sol(s)	ID	Camera	View Direction	Feature Name	Category
1		R13-03051, R13-01467, R20-01024	MOC-NA			
2a	6–10	2P127074636FFL0211P2215L2M3	Pancam	NE	Mission Success Pan	bedforms
2a	6–10	2P127090410FFL0211P2216L2M3	Pancam	NE	Mission Success Pan	bedforms
2a	6–10	2P127248269FFL0211P2216L2M2	Pancam	NE	Mission Success Pan	bedforms
2a	6–10	2P127247698FFL0211P2216L2M2	Pancam	NE	Mission Success Pan	bedforms
2b	290	2P152107547FFL8987P2542L4M1	Pancam			windtails
2c	107	2P135858857FFL3100P2554L2M1	Pancam		Wallula Gap	ventifact w/grooves
2d	73	2P132838578SFL2000P2559L2M1	Pancam		White Elephant	ventifact w/grooves, close-up
2e	108	2P135942564FFL3200P2392L2M1	Pancam		Midfield Rock Survey	two-tone
2f	60	2P131696667FFL1159P2597L2M1	Pancam		Humphrey	RAT tail
2g	89	2P134260621FFL2400P2533L2M1	Pancam		tracks	dark soil
3a	69	2P132489576FFL1800P2289L2M1	Pancam	SE	Bonneville Pan	hollow and bedforms
3a	69	2P132490971FFL1800P2289L2M1	Pancam	SE	Bonneville Pan	hollow and bedforms
3a	69	2P132491257FFL1800P2289L2M1	Pancam	SE	Bonneville Pan	hollow and bedforms
3a	69	2P132485775FFL1800P2290L2M1	Pancam	SE	Bonneville Pan	hollow and bedforms
3a	69	2P132486067FFL1800P2290L2M1	Pancam	SE	Bonneville Pan	hollow and bedforms
3a	69	2P132489850FFL1800P2289L2M1	Pancam	SE	Bonneville Pan	hollow and bedforms
3a	69	2P132490691FFL1800P2289L2M1	Pancam	SE	Bonneville Pan	hollow and bedforms
3a	69	2P132491555FFL1800P2289L2M1	Pancam	SE	Bonneville Pan	hollow and bedforms
3a	69	2P132485659FFL1800P2290L2M1	Pancam	SE	Bonneville Pan	hollow and bedforms
3a	69	2P132483380FFL1800P2290L2M1	Pancam	SE	Bonneville Pan	hollow and bedforms
3b	53	2P131080679FFL1124P2573L2M1	Pancam		Toad	rock surrounded by windtails
3c	56	2P131347008FFL1155P2584L2M1	Pancam		Photometry sequence	ripples (with small windtails)
3d	99	2P135156114FFL2700P2542L2M1	Pancam		Orel	facet
3e	87	2P134101174SFL2300P2460L2M1	Pancam		Systematic Soil Survey	grooves (into soil)
3f	63	2P131954806SFL1300P2532L2M1	Pancam		Orca	Perched Rock and grooves
4a	100	2N135241174EFF2702P1959L0M1	Navcam		Route 66	Grooves
4b	52	2M130974187EFF1100P2953M2F1	Micro-Imager		Sugar T	dusty grains
4c	46	2M130463334EFF0900P2953M2F1	Micro-Imager		Trout 1	poor sorted grains
4d	90	2P134352572EFF2500P2514R1C1	Pancam		Clast Survey	broken slab
4e	130	2P137912072ESF5000P2575L2C1	Pancam		Don't Tread on Me/Tracks	dark soil
5a	39	2F129834922EFF0500P1210L0M1	Front Hazcam		Drifter	bedform
5b	39	2M129820929EFF0400P2943L0M1	Micro-Imager		Squiggle	bedform
5c	40	2F129914137EFF0506P1210L0M1	Front Hazcam		Arena	bedform
5d	41	2M130001298EFF0506P2943L0M2	Micro-Imager		Crest - Arena	bedform
5e	41	2M130001885EFF0506P2943L0M1	Micro-Imager		Trough - Arena	bedform
5f	44	2F130264571EFF0700P1120L0M1	Front Hazcam		Flats	plains
5g	44	2M130267583EFF0700P2938L0M1	Micro-Imager		Ramp Flats	matrix supported clasts
8	111	2N136235243EFF3600P1846L0M1	Navcam		Navcam Pan	bedform
8	111	2N136234863EFF3600P1818L0M1	Navcam		Navcam Pan	bedform
10a	71	2F132673311EFF18AAP1201L0M1	Front Hazcam		Serpent	bedform
10b	72	2P132756681EFF1957P2352L2C1	Pancam		Bear Paw - Serpent	bedform
10b	72	2P132756270EFF1957P2352L2C1	Pancam		Bear Paw - Serpent	bedform
10c	73	2M132840805EFF2000P2937M2F1	Micro-Imager		Serpent	bedform
10d	73	2M132841379EFF2000P2977M2F1	Micro-Imager		Serpent	bedform
10e	73	2M132842058EFF2000P2977M2F1	Micro-Imager		Serpent	bedform
10f	73	2M132842726EFF2000P2977M2F1	Micro-Imager		Serpent	bedform
11	290	2P152107603FFL8987P2542L6M1	Pancam			windtails
12	41	2P129997661EFF0506P2534L2C1	Pancam		Axe	bedform superposed on windtails
13a	16	2P127783908EFF0327P2370L7M1	Pancam		Adirondack	facet
13b	76	2P133107031ESF2200P2567L3C1	Pancam		Mazatzal	facet and grooves
13c	78	2P133290550FFL2232P2359L7M1	Pancam		Bonneville Crater Pan	facets
13d	310	2P153892840FFL91C0P2426L7M1	Pancam		Drive Direction Pan	facets
13e	58	2P131526768FFL1155P2437L7M1	Pancam		Frontier	grooved facet
13f	88	2P134172259EFF2300P2450L4C1	Pancam		Systematic Soil Survey	grooved facet
14	63	2P131954334SFL1300P2531R1M1	Pancam		Orca	grooved terrace rock
15a	88	2P134183912FFL2400P2372L7M1	Pancam		Drive Direction	Perched Rock
15b	41	2P129999373FFL0506P2531R2M1	Pancam		Gepetto	Perched Rock
15c	65	2N132143228FFL1600P1835L0M1	Navcam		Navcam Pan	Perched Rock
15d	108	2P135943222FFL3200P2392C2M1	Pancam		Midfield Rock Survey	Perched Rock
15e	68	2P132404360FFL1800P2286L2M1	Pancam		Bonneville Crater Pan	Perched Rock
17a		434S07	Viking		Gusev Crater	
17b		434S07	Viking		MER-A landing ellipse in Gusev	
17c		434S07	Viking		Bright streaks	bright streaks
17d		M10-03184	MOC-NA		Dark Streak	dark streak
17e		M07-00813	MOC-NA		Dark Streaks - slope break	dark streak
17f		R07-01606	MOC-NA		Dark Streaks	dark streak - few km N of LS
17g		M03-01042	MOC-NA		Dunes	transverse dunes
19a	496	2N170391683SFLAAFQP1560L0M1	Navcam		Navcam Dust Devil Movie	dust devil
19b	489	2N169770718SFLAAEOP1560L0M1	Navcam		Navcam Dust Devil Movie	dust devil
20a	59	2P131613980SFL1155P2592L7M1	Pancam		Humphrey	RAT tail
20b	35	2N129477093FFL0327P1635L0M1	Navcam		Adirondack	RAT tail

Table A1. (continued)

Figure	Sol(s)	ID	Camera	View Direction	Feature Name	Category
20c	200	2P144127789FFL7602P2556L2M1	Pancam		Wooly Patch	RAT tail
21a	350	2M157437650EFFA225P2936M2M1	Micro-Imager		Deck	active grains
21b	431	2M164620654EFFA8B3P2936M2M1	Micro-Imager		Deck	active grains
21c	505	2M171194380EFFAAIIP2959M2M1	Micro-Imager		Deck	active grains
21d	505	2N171194271FFLAAIIP1938L0M1	Navcam		IDD on deck	

[62] 4. Do the ventifacts represent current conditions, or were they cut by processes in the past when conditions for wind abrasion might have been more favorable?

[63] 5. There is an inconsistency in the orientations of the facets and the grooves in the Columbia Hills. If both types of features represent wind abrasion, why do they not indicate the same wind directions?

[64] 6. What are the timescales of the features observed? Although the dark linear wind streaks are shown to form currently, when did the dunes and ripples develop? If they represent previous conditions, how long ago might they have formed and why was there a shift to current conditions?

[65] Some of these issues can be addressed with further reduction and analysis of available data. In other cases, such as determining the timescales of events not only in Gusev crater but elsewhere on Mars, new data will need to be obtained.

Appendix A

[66] Most of the analysis of wind-related features is based on imaging data from Spirit. Table A1 lists the key parameters for the images used in the figures, and includes the sol on which the image was taken, the camera system, the informal names applied by the MER team, and the category of feature illustrated.

[67] **Acknowledgments.** We thank Danny Foley, Michael Bentley, Stephanie Holaday, and Charles Hewett (all of ASU) for technical support of this investigation. P. Whelley and S. D. Thompson were partly supported by the NASA Space Grant Program at ASU. We thank Lori Fenton and an anonymous reviewer for extensive suggestions that enabled significant improvements to the manuscript. This work was performed for the Jet Propulsion Laboratory, California Institute of Technology, sponsored by the National Aeronautics and Space Administration.

References

Arvidson, R. E., et al. (2004), Localization and physical properties experiments conducted by Spirit at Gusev crater, *Science*, *305*, 821–824.

Arvidson, R. E., et al. (2006), Overview of the Spirit Mars Exploration Rover Mission to Gusev Crater: Landing site to Backstay Rock in the Columbia Hills, *J. Geophys. Res.*, *111*, E02S01, doi:10.1029/2005JE002499.

Bell, J. F., III, et al. (2003), Mars Exploration Rover Athena Panoramic Camera (Pancam) investigation, *J. Geophys. Res.*, *108*(E12), 8063, doi:10.1029/2003JE002070.

Bridges, N. T., R. Greeley, A. F. C. Haldemann, K. E. Herkenhoff, M. Kraft, T. J. Parker, and A. W. Ward (1999), Ventifacts at the Pathfinder landing site, *J. Geophys. Res.*, *104*, 8595–8615.

Bridges, N. T., J. E. Laity, R. Greeley, J. Phoreman, and E. E. Eddlemon (2004), Insights on rock abrasion and ventifact formation from laboratory and field analog studies with applications to Mars, *Planet. Space Sci.*, *521*, 199–213.

Cabrol, N. A., et al. (2003), Exploring Gusev Crater with Spirit: Review of science objectives and testable hypotheses, *J. Geophys. Res.*, *108*(E12), 8076, doi:10.1029/2002JE002026.

Christensen, P. R., et al. (2003), Miniature Thermal Emission Spectrometer for the Mars Exploration Rovers, *J. Geophys. Res.*, *108*(E12), 8064, doi:10.1029/2003JE002117.

Christensen, P. R., et al. (2004a), Initial results from the Mini-TES experiment in Gusev crater from the Spirit Rover, *Science*, *305*, 837–842.

Christensen, P. R., et al. (2004b), The thermal emission imaging system (THEMIS) for the Mars 2001 Odyssey mission, *Space Sci. Rev.*, *110*, 85–130.

Dutro, J. T., R. V. Dietrich, and R. M. Foose (1989), *AGI Data Sheets*, Am. Geol. Inst., Alexandria, Va.

Fergason, R. L., P. R. Christensen, J. F. Bell III, M. P. Golombek, K. Herkenhoff, H. H. Kieffer, and R. Sullivan (2006), Physical properties of the Mars Exploration Rover landing sites as inferred from Mini-TES derived thermal inertia, *J. Geophys. Res.*, doi:10.1029/2005JE002583, in press.

Gellert, R., et al. (2004), Chemistry of rocks and soils in Gusev crater from the Alpha Particle X-ray Spectrometer, *Science*, *305*, 829–832.

Gellert, R., et al. (2006), The Alpha Particle X-Ray Spectrometer (APXS): Results from Gusev crater and calibration report, *J. Geophys. Res.*, doi:10.1029/2005JE002555, in press.

Gillette, D. A., and P. H. Stockton (1989), The effect of nonerodible particles on wind erosion of erodible surfaces, *J. Geophys. Res.*, *94*, 12,885–12,893.

Golombek, M. P., et al. (2003), Selection of the Mars Exploration Rover landing sites, *J. Geophys. Res.*, *108*(E12), 8072, doi:10.1029/2003JE002074.

Golombek, M. P., et al. (2005), Assessment of Mars Exploration Rover landing site predictions, *Nature*, *436*, 44–48.

Golombek, M. P., et al. (2006), Geology of the Gusev cratered plains from the Spirit rover transverse, *J. Geophys. Res.*, doi:10.1029/2005JE002503, in press.

Gorevan, S. P., et al. (2003), Rock Abrasion Tool: Mars Exploration Rover mission, *J. Geophys. Res.*, *108*(E12), 8068, doi:10.1029/2003JE002061.

Goudie, A. S., R. U. Cooke, and J. C. Doornkamp (1979), The formation of silt from quartz dune sand by salt-weathering processes in deserts, *J. Arid Environ.*, *2*, 105–112.

Grant, J. A., and P. A. Schultz (1987), Possible tornado-like tracks on Mars, *Science*, *237*, 883–885.

Grant, J. A., et al. (2004), Surficial deposits at Gusev crater along Spirit rover traverses, *Science*, *305*, 807–810.

Grant, J. A., et al. (2006), Crater gradation in Gusev crater and Meridiani Planumm, Mars, *J. Geophys. Res., 111,* E02S08, doi:10.1029/2005JE002465.

Greeley, R., and J. D. Iversen (1985), *Wind as a Geological Process: Earth, Mars, Venus, and Titan*, 333 pp., Cambridge University Press, New York.

Greeley, R., and M. Kraft (2001), Survivability of aggregate sands on Mars, *Proc. Lunar Planet. Sci. Conf. 32nd*, 1839.

Greeley, R., R. N. Leach, S. H. Williams, B. R. White, J. B. Pollack, D. H. Krinsley, and J. R. Marshall (1982), Rate of wind abrasion on Mars, *J. Geophys. Res.*, *87*, 10,009–10,024.

Greeley, R., M. Kraft, R. Sullivan, G. Wilson, N. Bridges, K. Herkenhoff, R. O. Kuzmin, M. Malin, and W. Ward (1999), Aeolian features and processes at the Mars Pathfinder landing site, *J. Geophys. Res.*, *104*, 8573–8584. (Correction, *J. Geophys. Res.*, *104*, 22,065, 1999.)

Greeley, R., M. D. Kraft, R. O. Kuzmin, and N. T. Bridges (2000), Mars Pathfinder landing site: Evidence for a change in wind regime from lander and orbiter data, *J. Geophys. Res.*, *105*, 1829–1840.

Greeley, R., N. T. Bridges, R. O. Kuzmin, and J. E. Laity (2002), Terrestrial analogs to wind-related features at the Viking and Pathfinder landing sites on Mars, *J. Geophys. Res.*, *107*(E1), 5005, doi:10.1029/2000JE001481.

Greeley, R., R. O. Kuzmin, S. C. R. Rafkin, T. I. Michaels, and R. Haberle (2003), Wind-related features in Gusev crater, Mars, *J. Geophys. Res.*, *108*(E12), 8077, doi:10.1029/2002JE002006.

Greeley, R., et al. (2004), Wind-related processes detected by the Spirit Rover at Gusev crater, Mars, *Science*, *305*, 810–821.

Greeley, R., B. H. Foing, H. Y. McSween Jr., G. Neukum, P. Pinet, M. van Kan, S. C. Werner, D. A. Williams, and T. E. Zegers (2005a), Fluid lava flows in Gusev crater, Mars, *J. Geophys. Res.*, 110, E05008, doi:10.1029/2005JE002401.

Greeley, R., et al. (2005b), Martian variable features: New insight from the Mars Express Orbiter and the Mars Exploration Rover Spirit, *J. Geophys. Res.*, *110*, E06002, doi:10.1029/2005JE002403.

Haberle, R. M., J. B. Pollack, J. R. Barnes, R. W. Zurek, C. B. Leovy, J. R. Murphy, H. Lee, and J. Schaeffer (1993), Mars atmospheric dynamics as simulated by the NASA-Ames general circulation model: 1. The zonal mean circulation, *J. Geophys. Res.*, *98*, 3093–3123.

Herkenhoff, K. E., et al. (2003), Athena Microscopic Imager investigation, *J. Geophys. Res.*, *108*(E12), 8065, doi:10.1029/2003JE002076.

Herkenhoff, K. E., et al. (2004), Textures of the soils and rocks at Gusev crater from Spirit's Microscopic Imager, *Science*, *305*, 824–826.

Kuzmin, R. O., R. Greeley, R. Landheim, N. A. Cabrol, and J. D. Farmer (2000), Geological map of the MTM-15,182 and -15,187 Quadrangles, Gusev crater–Ma'adim Vallis region, Mars, *U.S. Geol. Surv. Misc. Geol. Invest. Map*, *I-2666*.

Lemmon, M. T., et al. (2004), Atmospheric imaging results from the Mars Exploration Rovers: Spirit and Opportunity, *Science*, *306*, 1753–1756.

Li, R. (2005), l results of rover localization and topographic mapping for the 2003 Mars Exploration Rover mission, *J. Photogramm. Eng. Remote Sens.*, *71*, 1129–1142.

Livingstone, I., and A. Warren (1996), *Aeolian Geomorphology: An Introduction*, 221 pp., Addison-Wesley, Boston, Mass.

Maki, J. N., et al. (2003), Mars Exploration Rover Engineering Cameras, *J. Geophys. Res.*, *108*(E12), 8071, doi:10.1029/2003JE002077.

Malin, M. C., and K. Edgett (2001), Mars Global Surveyor Mars Orbiter Camera: Interplanetary cruise through primary mission, *J. Geophys. Res.*, *106*, 23,429–23,570.

McSween, H. Y., et al. (2004), Basaltic rocks analyzed by the Spirit Rover in Gusev crater, *Science*, *305*, 842–845.

Ming, D. W., et al. (2006), Geochemical and mineralogical indicators for aqueous processes in the Columbia Hills of Gusev crater, *J. Geophys. Res.*, doi:10.1029/2005JE002560, in press.

Morris, R. V., et al. (2004), Mineralogy at Gusev crater from the Mossbauer spectrometer on the Spirit rover, *Science*, *305*, 833–836.

Morris, R. V., et al. (2006), Mossbauer mineralogy of rock, soil, and dust at Gusev crater, Mars: Spirit's journey through weakly altered olivine basalt on the plains and pervasively altered basalt in the Columbia Hills, *J. Geophys. Res.*, doi:10.1029/2005JE002584, in press.

Neakrase, L. D. V., R. Greeley, and D. Foley (2004), Mars Exploration Rovers: Laboratory simulations of aeolian interactions, *Proc. Lunar Planet. Sci. Conf. 35th*, *1402*.

Neugebauer, G., G. Münch, H. Kieffer, S. C. Chase Jr., and E. Miner (1971), Mariner 1969 infrared radiometer results: Temperature and thermal properties of the Martian surface, *Astron. J.*, *76*, 719–728.

Neukum, G., R. Jaumann, and the HRSC Co-Investigator Team (2004), HRSC: The high resolution stereo camera of Mars Express, in *Mars Express: The Scientific Payload*, *Spec. Publ. SP-1240*, pp. 17–36, Eur. Space Agency, Noordwijk, Netherlands.

Nickling, W. G., and C. McKenna Neuman (1995), Development of deflation lag surfaces, *Sedimentology*, *42*, 403–414.

Pettijohn, F. J., P. E. Potter, and R. Siever (1987), *Sand and Sandstone*, Springer, New York.

Pollack, J. B. D., R. M. Haberle, J. Schaeffer, and H. Lee (1990), Simulations of the general circulation of the Martian atmosphere: 1. Polar processes, *J. Geophys. Res.*, *95*, 1447–1474.

Presley, M. A., and P. R. Christensen (1997), Thermal conductivity measurements of particulate materials: 2. Results, *J. Geophys. Res.*, *102*, 6551–6566.

Putzig, N. E., M. T. Mellon, K. A. Kretke, and R. E. Arvidson (2005), Global thermal inertia and surface properties of Mars from the MGS mapping mission, *Icarus*, *173*, 325–341.

Pye, K. (1987), *Aeolian Dust and Deposits*, 334 pp., Elsevier, New York.

Pye, K., and H. Tsoar (1990), *Aeolian Sand and Sand Dunes*, 396 pp., CRC Press, Boca Raton, Fla.

Rafkin, S. C. R., and T. I. Michaels (2003), Meteorological predictions for 2003 Mars Exploration Rover high-priority landing sites, *J. Geophys. Res.*, *108*(E12), 8091, doi:10.1029/2002JE002027.

Rafkin, S. C. R., R. M. Haberle, and T. I. Michaels (2001), The Mars Regional Atmospheric Modeling System: Model description and selected simulations, *Icarus*, *151*, 228–256.

Raupach, M. R., D. A. Gillette, and J. F. Leyes (1993), The effect of roughness elements on wind erosion threshold, *J. Geophys. Res.*, *98*, 3023–3029.

Sharp, R. P. (1963), Wind ripples, *J. Geol.*, *71*, 617–636.

Smith, D. E., and M. T. Zuber (1998), The relationship between MOLA Northern Hemisphere topography and the 6.1 mbar atmospheric pressure of Mars, *Geophys. Res. Lett.*, *25*, 4397–4400.

Smith, P. H., et al. (1997), Results from the Pathfinder camera, *Science*, *278*, 1758–1765.

Squyres, S. W., et al. (2004), The Spirit Rover Athena's science investigation at Gusev crater, Mars, *Science*, *305*, 794–799.

Squyres, S. W., et al. (2006), Rocks of the Columbia Hills, *J. Geophys. Res.*, doi:10.1029/2005JE002562, in press.

Wentworth, C. K. (1922), A scale of grade and class terms for clastic sediments, *J. Geol.*, *30*, 377–392.

Yen, A. S., et al. (2005), An integrated view of the chemistry and mineralogy of Martian soils, *Nature*, *436*, doi:10.1038/nature03637, 49–54.

R. E. Arvidson, Earth and Planetary Sciences, Washington University, St. Louis, MO 63130, USA. (arvidson@wunder.wustl.edu)

P. W. Barlett, Honeybee Robotics, 460 W 34th Street, New York, NY 10001, USA. (bartlett@honeybeerobotics.com)

D. Blaney, M. P. Golombek, and J. N. Maki, Jet Propulsion Laboratory, California Institute of Technology, 4800 Oak Grove Drive, Pasadena, CA 91109, USA. (diana.blaney@jpl.nasa.gov; mgolombek@jpl.nasa.gov)

N. A. Cabrol, NASA Ames Research Center, MS 245-3, Moffett Field, CA 94035-1000, USA. (ncabrol@mail.arc.nasa.gov)

P. R. Christensen, R. L. Fergason, R. Greeley, L. D. V. Neakrase, S. D. Thompson, and P. L. Whelley, Department of Geological Sciences, Box 871404, Tempe, AZ 85287-1404, USA. (phil.christensen@asu.edu; robin.fergason@asu.edu; greeley@asu.edu; shane.d.thompson@asu.edu; pwhelley@asu.edu)

P. A. de Souza Jr. CVRD Group, 29090-900 Vitória, ES, Brazil. (pasouza03@yahoo.com.br)

G. A. Landis, NASA Glenn Research Center, MS 302-1, Cleveland, OH 44135, USA. (geoffrey.a.landis@nasa.gov)

M. T. Lemmon, Department of Atmospheric Sciences, Texas A&M University, College Station, TX 77843, USA. (lemmon@tamu.edu)

S. M. McLennan, Department of Geosciences, State University of New York at Stony Brook, Stony Brook, NY 11794-2100, USA. (scott.mclennan@sunysb.edu)

T. Michaels and S. C. R. Rafkin, Southwest Research Institute, 1050 Walnut Street, Suite 400, Boulder, CO 80302, USA. (tmichael@boulder.swri.edu; srafkin@boulder.swri.edu)

J. E. Moersch, Department of Earth and Planetary Sciences, University of Tennessee, 1412 Circle Drive, Rm. 306, Knoxville, TN 37996, USA. (jmoersch@utk.edu)

L. Richter, Institut für Raumsimulation, Deutschen Zentrum für Luft- und Raumfahrt (DLR), D-51170 Köln, Germany. (lutz.richter@dlr.de)

S. W. Squyres and R. J. Sullivan, Department of Astronomy, Space Sciences Building, Cornell University, Ithaca, NY 14853, USA. (squyres@astro.cornell.edu; rjs33@cornell.edu)